An Electrochemical Model of the Transport of Charged Molecules through the Capillary Glycocalyx

T. M. Stace* and E. R. Damiano†

*Department of Physics, University of Western Australia, Perth, Australia; and †Department of Mechanical and Industrial Engineering, University of Illinois at Urbana-Champaign, Urbana, Illinois 61801 USA

ABSTRACT An electrochemical theory of the glycocalyx surface layer on capillary endothelial cells is developed as a model to study the electrochemical dynamics of anionic molecular transport within capillaries. Combining a constitutive relationship for electrochemical transport, derived from Fick's and Ohm's laws, with the conservation of mass and Gauss's law from electrostatics, a system of three nonlinear, coupled, second-order, partial, integro-differential equations is obtained for the concentrations of the diffusing anionic molecules and the cations and anions in the blood. With the exception of small departures from electroneutrality that arise locally near the apical region of the glycocalyx, the model assumes that cations in the blood counterbalance the fixed negative charges bound to the macromolecular matrix of the glycocalyx in equilibrium. In the presence of anionic molecular tracers injected into the capillary lumen, the model predicts the size- and charge-dependent electrophoretic mobility of ions and tracers within the layer. In particular, the model predicts that anionic molecules are excluded from the glycocalyx at equilibrium and that the extent of this exclusion, which increases with increasing tracer and/or glycocalyx electronegativity, is a fundamental determinant of anionic molecular transport through the layer. The model equations were integrated numerically using a Crank-Nicolson finite-difference scheme and Newton-Raphson iteration. When the concentration of the anionic molecular tracer is small compared with the concentration of ions in the blood, a linearized version of the model can be obtained and solved as an eigenvalue problem. The results of the linear and nonlinear models were found to be in good agreement for this physiologically important case. Furthermore, if the fixed-charge density of the glycocalyx is of the order of the concentration of ions in the blood, or larger, or if the magnitude of the anionic molecular valence is large, a closed-form asymptotic solution for the diffusion time can be obtained from the eigenvalue problem that compares favorably with the numerical solution. In either case, if leakage of anionic molecules out of the capillary occurs, diffusion time is seen to vary exponentially with anionic valence and in inverse proportion to the steady-state anionic tracer concentration in the layer relative to the lumen. These findings suggest several methods for obtaining an estimate of the glycocalyx fixed-charge density in vivo.

INTRODUCTION

The surface glycocalyx on capillary endothelial cells has been the subject of considerable controversy and conjecture in the recent literature on the microcirculation. The focus of much of this attention has been on the mechanical implications of the glycocalyx on microvascular rheology, specifically in terms of its gross effect on capillary tube hematocrit and apparent viscosity (Klitzman and Duling, 1979; Desjardins and Duling, 1990; Vink and Duling, 1996; Damiano et al., 1996; Pries et al., 1997; Damiano, 1998; Secomb et al., 1998). Very little emphasis, however, has been placed on the possible role of the glycocalyx in determining the electrophoretic mobility of charged molecules within capillaries. In light of recent experimental evidence (Vink and Duling, 2000), it appears as if significant electrostatic interactions arise between the glycocalyx and anionic molecular tracers which dramatically influence transport of the tracers. The potential significance of these findings to microvascular permeability and exchange motivates the present analysis of electrochemical molecular transport through the capillary glycocalyx.

Although the composition and structure of the endothelial-cell glycocalyx are not well characterized, insight into its mechanical and electrochemical behavior can be gained from what is known about some of its possible macromolecular constituents. It appears that these constituents include, but are not limited to, heparan sulfate proteoglycan, chondroitin sulfate proteoglycan, and hyaluronic acid (Desjardins and Duling, 1990; Henry and Duling, 1999). In this way, the endothelial-cell glycocalyx is similar to mucopolysaccharide structures arising in other systems (e.g., articular cartilage, tectorial membrane, etc.). This similarity essentially pertains to the fact that these mucopolysaccharide structures are highly hydrated in an electrolytic solution and are rich in proteoglycan, glycoprotein, and glycosaminoglycan (GAG) aggregates, which contain large numbers of solid-bound fixed negative charges. It also appears likely that the molecular composition of the glycocalyx varies across its thickness, from the endothelial-cell surface to its apical region within the capillary lumen. Henry and Duling (1999) found, through enzymatic reduction of the capillary glycocalyx with hyaluronidase, that hyaluronan (and perhaps other constituents that are cleaved by hyaluronidase) may contribute significantly to the apical glycocalyx. This

Received for publication 15 September 2000 and in final form 11 January 2001.

Address reprint requests to Dr. E. R. Damiano, Dept. of Mechanical and Industrial Engineering, University of Illinois at Urbana-Champaign, 140 Mechanical Engineering Bldg., 1206 West Green St., Urbana, IL 61801. Tel.: 217-333-6107; Fax: 217-244-6534; E-mail: damiano@uiuc.edu.

0006-3495/01/04/1670/21 $2.00

finding was based on the fact the very large dextran molecules, having molecular weights (MW) >580, and red cells remained excluded by the apical glycocalyx; yet smaller dextran molecules, <145 kDa, permeated significantly into the layer after enzymatic reduction with hyaluronidase. They also reported a marked increase in capillary tube hematocrit after hyaluronidase treatment, suggesting that the permeability of the glycocalyx to blood plasma is strongly dependent upon the presence of those constituents that are cleaved by hyaluronidase (Damiano, 1998; Secomb et al., 1998).

Combining intravital brightfield and fluorescence microscopy of the capillary glycocalyx, Duling and co-workers (Vink and Duling, 1996, 2000; Henry and Duling, 1999) have revealed its surprisingly large in vivo dimension, its unexpected permeability properties, and the tenuous nature of its structure. They have also shown that the illumination used to visualize the layer also results in its eradication if epifluorescent exposure is sustained for >3–5 min. Their approach consists essentially of obtaining two images—one brightfield image of a capillary using transillumination, and one image of fluorescently labeled tracers in the capillary lumen using epifluorescence illumination an instant later. By subtracting the width of the fluorescent tracer column from the anatomical diameter of the capillary imaged under transillumination, one has a measure of either the instantaneous in vivo thickness of glycocalyx, if the tracers are sufficiently large so as to be excluded by the layer, or the extent of diffusion into the layer of tracers small enough to penetrate the glycocalyx pores. Using this technique, Vink and Duling (1996, 2000) concluded that the in vivo thickness of the glycocalyx was $\sim 0.4-0.5\ \mu$m. This represents a much more substantial structure than previous estimates derived from electron microscopy studies, which likely underestimate the thickness due to dehydration of the extracellular matrix that inevitably accompanies tissue fixation. Consequently, on the basis of these electron microscopy studies, estimates of the glycocalyx thickness on capillary endothelial cells were on the order of only 50–100 nm. It is for this reason, perhaps, more than any other, that the glycocalyx has been almost entirely overlooked in matters concerning microvascular rheology, permeability, and exchange.

Because the capillary glycocalyx is at the interface between blood and the luminal endothelial-cell surface, it represents the first barrier to transvascular exchange. It is evident, therefore, that microvascular permeability is dependent upon glycocalyx permeability. To probe this, Vink and Duling (2000) conducted a series of experiments to study glycocalyx permeability within capillaries. They observed that dextran molecules >70 kDa remained excluded from the glycocalyx by virtue of their size for over 3 h, regardless of whether they were labeled with anionic or neutral fluorescent dyes. However, smaller anionic dextrans between 4 and 40 kDa invaded the glycocalyx with size-dependent half-times of between 12 and 60 min, respectively. Even extremely small anionic dyes between 0.4 and 0.6 kDa showed half-times of 11 min. Alternatively, neutral dyes of $\sim$0.4 kDa and neutral dextrans of <40 kDa equilibrated within one capillary transit time. For neutral dextran molecules <40 kDa, the corresponding Fickian diffusion time in plasma over the glycocalyx length scale of $\sim 0.4\ \mu$m is <20 ms. Thus, diffusion times for charged molecules could potentially be as much as five orders of magnitude longer than their neutral counterparts. These results suggest an important role for the solid-bound fixed charges of the glycocalyx matrix in capillary permeability.

It is in the midst of this rather unsettled state of affairs that we find ourselves without adequate quantitative explanations for many of these recent experimental findings. In an attempt to close this gap between experimental observation and theoretical understanding, we embark upon an electrochemical analysis of the glycocalyx that is sophisticated enough to address the salient physical phenomena while avoiding contrived specificity. We seek to determine whether a relatively simple electrochemical model of the glycocalyx can account for the disparity in diffusion times between anionic and neutral molecular tracers reported by Vink and Duling (2000). The model assumes that the glycocalyx consists of a multicomponent mixture that includes a fluid constituent (blood plasma), mobile ions (cations and anions), and a solid proteoglycan/glycoprotein/GAG matrix containing fixed negative charges. The negative charges bound to the solid matrix are assumed to have a fixed-charge distribution in the reference configuration given by $|z^F c^F(\boldsymbol{x}, t_0)|$, where z^F and c^F are, respectively, the mean valence and concentration distribution associated with the molecular constituents of the glycocalyx. In equilibrium, it is expected that the mobile ions establish a distribution that nearly counterbalances the fixed charges on the solid matrix such that a state of electroneutrality exists throughout the vessel, except for a slight departure localized near the apical glycocalyx, i.e., near the interface between the glycocalyx and vessel lumen. When integrated over the vessel cross section, however, these local charge imbalances should cancel such that global space-charge neutrality exists within the capillary. Therefore, throughout the vessel lumen where there is no glycocalyx, the concentration distributions of mobile anions and cations should be equal. The mobile ions in this region can be thought of as a neutral salt (Lai et al., 1991), which has no net effect on the total charge density within the capillary. However, near the glycocalyx interface, the mobile cation concentration is expected to increase to nearly neutralize the fixed negative charges on the glycocalyx, while the mobile anion concentration should decrease. These concentration gradients in the mobile ion distributions must be supported in equilibrium by the electric field generated by the glycocalyx. As we shall see, this electric field exerts its effect on the diffusing anionic molecular tracers by partially excluding them from the glyco-

calyx. The degree to which this exclusion occurs is primarily dependent upon the molecular tracer valence and glycocalyx fixed-charge density.

In what follows, a constitutive relationship derived from Fick's and Ohm's laws is proposed for the electrochemical flux of an anionic molecular tracer. Together with the conservation of mass, Gauss's law from electrostatics, and appropriate boundary conditions, a closed model is obtained for electrochemical transport through the capillary glycocalyx. This model is solved numerically for the one-dimensional, axisymmetric, spatiotemporal concentration distributions of the molecular tracer and mobile ions in the blood. Furthermore, a linear analysis is developed which is valid whenever the molecular tracer concentration is small compared with the ion concentration in the blood. From this analysis, a closed-form asymptotic expression is derived for the molecular tracer diffusion time that is valid if either the fixed-charge density is large compared with the ion concentration in the blood or the electronegativity of the anionic molecular tracer is large. Following this is a discussion of analytical results where we consider specific parameter values (e.g., molecular tracer valence, glycocalyx fixed-charge density, and glycocalyx distribution) required to reproduce the recent experimental findings of Vink and Duling (2000). We conclude with a discussion of the model's implications for the system in equilibrium and propose several alternative experimental approaches to finding the glycocalyx fixed-charge density in vivo that are independent of molecular diffusion times or the reaction-diffusion kinetics of the system.

THE MODEL

The glycocalyx is modeled here as a continuously distributed anionic matrix made up of proteoglycans, glycoproteins, and GAGs containing fixed-bound negative charges through which a solution of anionic molecular tracers in blood plasma can diffuse. Of fundamental importance to the model is that it account for the presence of ionic salts (Na^+, Cl^-, etc.) in the blood. The validity of the continuum approximation used here for the glycocalyx matrix depends not only upon the instantaneous spatial distributions of the matrix and fixed charge groups, but also upon the temporal variations in those distributions arising from Brownian motion of the matrix. In fact, if it were not for these temporal variations, the continuum approximation might not be reasonable. In particular, we assume that in its hydrated state, the glycocalyx is extremely diffuse and resembles other collagen-poor mucopolysaccharide extracellular matrix structures with solid-volume fractions below 1% (Levick, 1987). The instantaneous fixed-charge distribution in such a structure is therefore likely to be quite heterogeneous. Furthermore, the Debye length in normal saline is <0.2 nm, and thus the electric field induced by the fixed charges bound to the glycocalyx is very efficiently shielded by the counter cations in the blood. At such high cation concentrations relative to c^f the strength of the electric field, at a distance of 1 nm or more from one of the fixed-charge groups, would be reduced to $<1\%$ of its maximum value if the glycocalyx matrix were a static scaffold with fixed-bound-negative charges. Indeed, if it were not for Brownian motion of the glycocalyx matrix itself, the instantaneous electric field distribution in a system with such a low solid-volume fraction and such a high cation concentration would likely be extremely nonuniform. However, when one accounts for Brownian motion of the proteoglycan/glycoprotein/GAG aggregates at 310 K, the time-averaged spatiotemporal distribution of the electric field would certainly be more uniform than the instantaneous distribution, making the continuum approach more reasonable. Therefore, we assume that variations in the electric field arising from cationic charge shielding and sparsity of the individual fixed charges bound to the glycocalyx matrix are offset, in a time-averaged sense, by Brownian motion of the matrix. We therefore model the glycocalyx as having a continuous concentration distribution and continuous fixed-charge density distribution (with at most a finite number of discontinuities at interfaces) such that spatial variations in the electric field are solely a result of spatial variations in the time-averaged fixed-charge density distribution.

By invoking the continuum approximation, we bring to bear the classical theory of electrochemical ionic transport in solution, which has its origins in the Nernst-Planck equation (Bockris and Reddy, 1970). In the context of this theory, transport is driven principally by chemical gradients and electrostatic forces. In the case of transport of anionic molecular tracers through the glycocalyx, the results of Vink and Duling (2000) suggest a strong dependence on tracer valence; thus, the important contributions to molecular transport that are considered here are derived from chemical and electrostatic potentials.

Conservation of mass

In the absence of chemical reactions, the time rate of change of the concentration, c^γ, of species γ is related to its flux, $\boldsymbol{J}^\gamma$, relative to a quiescent solvent, by the conservation equation given by

$$\frac{\partial c^\gamma}{\partial t} = -\boldsymbol{\nabla} \cdot \boldsymbol{J}^\gamma, \tag{1}$$

The various flux contributions mentioned above must be specified by appropriate constitutive relations.

Constitutive flux laws

For any mass transport problem there is a flux, $\boldsymbol{J}^\gamma_{\text{chemical}}$, associated with the chemical potential of the diffusing species that is proportional to the concentration gradients of the

species γ. Typically, this is modeled using Fick's law of diffusion. To account for the strong charge dependence in the results of Vink and Duling (2000), a flux, $\boldsymbol{J}^{\gamma}_{\text{electric}}$, due to electrostatic interactions of species γ with the electric field induced by the glycocalyx is also introduced. The constitutive flux law for electrostatically driven transport is derived from Ohm's law, and is obtained by considering electrostatic and viscous forces that act on a diffusing particle in suspension due to the effect of all charges in the system. Thus, we model the total electrochemical flux, $\boldsymbol{J}^{\gamma}$, of species γ as the sum of Fick's and Ohm's laws given by

$$\boldsymbol{J}^{\gamma} = \boldsymbol{J}^{\gamma}_{\text{chemical}} + \boldsymbol{J}^{\gamma}_{\text{electric}}, \tag{2}$$

$$= -D^{\gamma}\boldsymbol{\nabla}c^{\gamma} + \frac{z^{\gamma}q}{f^{\gamma}_{\text{d}}}c^{\gamma}\boldsymbol{E}, \tag{3}$$

where D^{γ} is the diffusion coefficient, z^{γ} is the ionic valence, f^{γ}_{d} is the Stokes drag coefficient, q is the elementary charge, and $\boldsymbol{E}$ is the electric field vector. This expression forms the basis for the model presented here. It should be noted that z^{γ} represents the effective valence, which provides the correct electrophoretic mobility of the charged molecule in solution. The effect of charge shielding is then accounted for in the valence, which may take on noninteger values.

Electrochemical transport equations

The Stokes drag coefficient, f^{γ}_{d}, is related to the diffusion coefficient according to the Einstein relation, $D^{\gamma} = k_{\text{B}}T/f^{\gamma}_{\text{d}}$, where k_{B} is Boltzmann's constant and T is the absolute temperature (Reif, 1965). Thus, the flux and species conservation equations become

$$\boldsymbol{J}^{\gamma} = -D^{\gamma}\left(\boldsymbol{\nabla}c^{\gamma} - \frac{z^{\gamma}q}{k_{\text{B}}T}c^{\gamma}\boldsymbol{E}\right), \tag{4}$$

$$\frac{\partial c^{\gamma}}{\partial t} = \boldsymbol{\nabla}\cdot\left(D^{\gamma}\boldsymbol{\nabla}c^{\gamma} - D^{\gamma}\frac{z^{\gamma}q}{k_{\text{B}}T}c^{\gamma}\boldsymbol{E}\right). \tag{5}$$

The index γ makes explicit the fact that there are different diffusing species in the system. Namely, γ may take the values $+$, $-$, and L, for the mobile cations (Na^{+}), the mobile anions (Cl^{-}), and anionic molecular tracers, respectively.

It remains now to determine the electric field $\boldsymbol{E}$ due to the presence of charge imbalances in the system. From the outset it should be noted that there will be global charge balance, so that the total charge in the system is zero. There may, however, be local charge imbalances due to gradients in the concentrations of the various species. The electric field due to a system of charges may be determined using Gauss's law from electrostatics. The divergence of the electric field depends on the local charge density, ρ, according to

$$\boldsymbol{\nabla}\cdot\boldsymbol{E} = \frac{\rho}{\varepsilon} \tag{6}$$

where ε is the permittivity of the surrounding medium, which is taken to be the same as that of water (1.57×10^{-11} F/m).

At this point, the effect of the glycocalyx may be included. The glycocalyx is assumed to be a charged porous matrix of macromolecules, each with valence z^{F}. The concentration of macromolecules in the glycocalyx is denoted by c^{F}, which varies over the cross section of the capillary. The glycocalyx fixed-charge density is then denoted by $|z^{\text{F}}c^{\text{F}}|$. In this analysis, deformations of the glycocalyx are considered negligible, so the initially specified concentration, c^{F}, does not vary with time. For convenience, we introduce the quantity $\delta = \rho/q$, which represents the local charge imbalance per unit charge and corresponds to the valence-weighted sum of constituent concentrations given by

$$\delta = z^{+}c^{+} + z^{-}c^{-} - nc^{\text{F}} - mc^{\text{L}}, \tag{7}$$

where, for convenience, we have introduced the parameters $m = -z^{\text{L}}$ and $n = -z^{\text{F}}$. Gauss's law, given in terms of δ by $\boldsymbol{\nabla}\cdot\boldsymbol{E} = q\delta/\varepsilon$, taken together with the three second-order, nonlinear, partial differential equations represented by Eq. 5, provide a system of four scalar equations in the four unknowns, $c^{+}(\boldsymbol{x}, t)$, $c^{-}(\boldsymbol{x}, t)$, $c^{\text{L}}(\boldsymbol{x}, t)$, and $\delta(\boldsymbol{x}, t)$.

Axisymmetric form of the equations

In all of what follows, axisymmetric conditions will be imposed and axial variations in the field variables will be neglected. With this approximation, all variables depend only on the radial coordinate, r, and time. This simplifies the governing equations substantially since Gauss's law is then integrable. Omitting uniform additive contributions to the electric field in the $\hat{e}_{\text{r}}$, $\hat{e}_{\varphi}$, and $\hat{e}_{\text{z}}$ directions, Eq. 6 reduces to

$$\frac{1}{r}\frac{\partial(rE_{\text{r}})}{\partial r} = \frac{q\delta}{\varepsilon} \Rightarrow E_{\text{r}} = \frac{q}{\varepsilon r}\int_{0}^{\text{r}}\delta(\sigma, t)\sigma\,\text{d}\sigma \tag{8}$$

where, by axisymmetry, the electric field has only a radial component such that $\boldsymbol{E} = E_{\text{r}}(r\,t)\hat{e}_{\text{r}}$. Furthermore, in the axisymmetric case, the electric field must vanish at $r = 0$. If there is zero net charge in the system, the electric field must also vanish at the system boundary at $r = \mathcal{R}$. This global electroneutrality condition requires that

$$E_{\text{r}}(\mathcal{R}) = \frac{q}{\varepsilon\mathcal{R}}\int_{0}^{\mathcal{R}}\delta(\sigma, t)\sigma\,\text{d}\sigma = 0. \tag{9}$$

The conservation equations contained in Eq. 5 may be written in cylindrical coordinates, and upon substitution of

Eq. 8 for E_r, they become

$$\frac{\partial c^\gamma}{\partial t} = \frac{1}{r}\frac{\partial}{\partial r}\left(D^\gamma r \frac{\partial c^\gamma}{\partial r} - \frac{D^\gamma z^\gamma q^2}{k_B T \varepsilon} c^\gamma \int_0^r \delta(\sigma, t)\sigma \, d\sigma \right) \quad (10)$$

for $\gamma = +, -$, and L. The fourth equation needed for closure is just the definition of δ given by Eq. 7. Thus, substitution of Eq. 7 into Eq. 10 provides a coupled system of three scalar, second-order, nonlinear, partial integro-differential equations in the three unknowns, c^+, c^-, and c^L.

Boundary conditions

Because the equations represented by Eq. 10 have one time derivative and two space derivatives, an initial condition and two boundary conditions are needed. For a closed system, the flux of any species across the system boundary must vanish. In particular, if the closed boundary of the system is at $r = \mathcal{R}$, then the radial component of the flux must satisfy $J_r^\gamma(\mathcal{R}, t) = 0$. Expressing Eq. 4 for the flux in axisymmetric cylindrical coordinates, this boundary condition takes the form

$$J_r^\gamma(\mathcal{R}, t) = -D^\gamma \left(\left.\frac{\partial c^\gamma}{\partial r}\right|_{r=\mathcal{R}} - \frac{z^\gamma q}{k_B T} c^\gamma E_r(\mathcal{R}) \right) = 0. \quad (11)$$

Recalling the charge balance requirement of Eq. 9, this boundary condition simplifies to

$$\left.\frac{\partial c^\gamma}{\partial r}\right|_{r=\mathcal{R}} = 0. \quad (12)$$

The second boundary condition arises from the geometry of the problem. Because the system is presumed to be axisymmetric, odd derivatives of the concentration vanish at $r = 0$, which provides the second boundary condition given by

$$\left.\frac{\partial c^\gamma}{\partial r}\right|_{r=0} = 0. \quad (13)$$

Initial conditions

We assume a Gaussian radial distribution for the initial concentration, $c^L(r, t_0)$, of molecular tracers. As we will see, the diffusion time is insensitive to the exact form of this initial distribution. However, the initial distributions of the mobile salt ions, Na^+ and Cl^-, present a more difficult problem. Because it is assumed that salts in the blood plasma are in equilibrium before molecular tracers are added, the condition that determines the initial c^+ and c^- distributions is that the flux vanish identically. Therefore, we must solve Eq. 4 subject to the constraint that $\boldsymbol{J}^\pm \equiv 0$. The electric field for these equations is given by Eq. 8, but with $c^L = 0$ in Eq. 7 defining δ. In cylindrical coordinates, the two zero-flux equations become

$$r\frac{dc^\pm}{dr} - \frac{z^\pm q^2 c^\pm}{k_B T \varepsilon} \int_0^r \delta(\sigma)\sigma \, d\sigma = 0, \quad (14)$$

and the expression for δ in equilibrium becomes

$$\delta(r) = z^+ c^+(r) + z^- c^-(r) - n c^F(r). \quad (15)$$

As for the unsteady case, the boundary conditions for Eq. 14 are given by Eqs. 12 and 13. From Eqs. 12–15, steady-state solutions can be obtained that represent the equilibrium configurations for $c^\pm(r, t_0)$ immediately before molecular tracers are added.

Nondimensional form of the equations

So that reasonable order-of-magnitude approximations can be made, we make the relative size of each term in the equations apparent by nondimensionalizing the variables and equations. The parameters that characterize the problem are given in Table 1. Using an asterisk to denote dimensionless variables, the dependent and independent variables are nondimensionalized as follows:

$$r = \mathcal{R} r^*, \quad t = \frac{\mathcal{R}^2}{(D^+ D^L)^{1/2}} t^*, \quad (16)$$

$$c^\pm = c_{blood} c^{\pm *}, \quad c^L = c_0^L c^{L*}, \quad c^F = c_0^F c^{F*}, \quad \delta = c_0^L \delta^*. \quad (17)$$

TABLE 1 Parameter values used in the model

Symbol	Description	Typical Value
c_0^L	Concentration of dextrans in blood	3.5×10^{-5} mol/l*
c_{blood}	Concentration of salts (Na^+, Cl^-) in blood	0.14 mol/l
$D^\pm$	Diffusion coefficient of Na^+ and Cl^- in water	10^{-9} m^2/s
D^L	Diffusion coefficient of molecular tracer in water	2.4×10^{-11} m^2/s*
$\mathcal{R}$	Radial dimension of entire system	3 − 10 μm
r_{ec}	Radial location of endothelial-cell surface	2.5 − 3 μm
$r_{ec} - r_g$	Thickness of glycocalyx	0.4 − 0.5 μm

*Values are typical for 39 kDa FITC-dextran tracers, but vary with molecular weight (see Table 2).

Taking D^{γ} to be constant, and assuming $D^{+} \approx D^{-}$, we have

$$\frac{\partial c^{\pm *}}{\partial t^*} = D\,\frac{1}{r^*}\,\frac{\partial}{\partial r^*}\left(r^*\,\frac{\partial c^{\pm *}}{\partial r^*} - z^{\gamma} Q c^{\pm *}\int_0^{r^*} \delta^*(\sigma^*)\sigma^*\,\mathrm{d}\sigma^*\right), \tag{18}$$

$$\frac{\partial c^{\mathrm{L}*}}{\partial t^*} = \frac{1}{D}\,\frac{1}{r^*}\,\frac{\partial}{\partial r^*}\left(r^*\,\frac{\partial c^{\mathrm{L}*}}{\partial r^*} - z^{\mathrm{L}} Q c^{\mathrm{L}*}\int_0^{r^*} \delta^*(\sigma^*)\sigma^*\,\mathrm{d}\sigma^*\right), \tag{19}$$

$$\delta^* = z^{+} B c^{+*} + z^{-} B c^{-*} - nF c^{\mathrm{F}*} - m c^{\mathrm{L}*}, \tag{20}$$

where we have introduced the following dimensionless groups:

$$Q = \frac{q^2 c_0^{\mathrm{L}} \mathcal{R}^2}{k_{\mathrm{B}} T \varepsilon}, \quad D = \left(\frac{D^{+}}{D^{\mathrm{L}}}\right)^{1/2}, \quad B = \frac{c_{\mathrm{blood}}}{c_0^{\mathrm{L}}}, \quad F = \frac{c_0^{\mathrm{F}}}{c_0^{\mathrm{L}}}. \tag{21}$$

Henceforth, the nondimensional form of the governing equations will be used, and for convenience, the asterisks will be dropped.

Glycocalyx distribution

The concentrations of proteoglycan, glycoprotein, and GAG macromolecules in the glycocalyx are assumed to increase continuously from zero in the lumen to a nearly constant (but unknown) value near the endothelial-cell wall. Leakage of the tracer molecules from the capillary into the extravascular space might also play an important role in the electrochemical dynamics. The glycocalyx distribution is thus approximated by an expression of the form:

$$c^{\mathrm{F}}(r) = \frac{\mathcal{N}}{4}\left(1 + \tanh\left(\frac{5.3}{\Delta r_{\mathrm{g}}}(r - r_{\mathrm{g}})\right)\right) \cdot \left(1 + \tanh\left(\frac{5.3}{\Delta r_{\mathrm{ec}}}(-r + r_{\mathrm{ec}})\right)\right)^{\dagger}. \tag{22}$$

The dagger indicates that the distribution is symmetrized about $r = 0$; that is, $p(r)^{\dagger} = p(r) + p(-r)$, and $\mathcal{N}$ is a scaling factor so that $\max\{c^{\mathrm{F}}(r)\} = 1$. The radii, r_{g} and r_{ec}, denote the locations of the lumen-glycocalyx and glycocalyx-endothelial boundaries, respectively, and are known approximately from experimental results of Vink and Duling (1996, 2000). Near r_{g}, 99% of the rise in c^{F} occurs over a distance Δr_{g}, while 99% of its fall occurs near r_{ec} over a distance Δr_{ec}. Fig. 1 shows a schematic diagram of this distribution. Setting both Δr_{g} and Δr_{ec} to zero results in a box-shaped distribution, with discontinuities in glycocalyx concentration at r_{g} and r_{ec}. In dimensional variables, the maximum concentration of the glycocalyx corresponds to c_0^{F}.

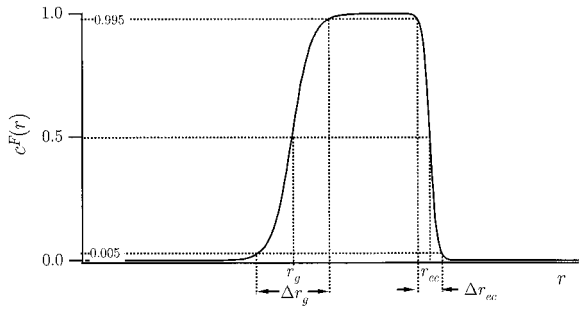

FIGURE 1 The assumed form of the c^{F} distribution, as in Eq. 22, showing the parameters r_{g}, Δr_{g}, r_{ec}, and Δr_{ec}. Not to scale.

EQUILIBRIUM CONFIGURATION

A few observations can be made about the three equations represented by Eqs. 18 and 19. They are clearly coupled through Eq. 20 for δ, and are nonlinear. The nonlinearity appears in the flux contribution associated with the electric potential, and is bilinear and quadratic. The integral term complicates the problem considerably because it means that local charge imbalances have global influence. Here we derive some exact and asymptotic relations of the equilibrium solutions, including an asymptotic expression for δ as a function of c^{F}. These results are used in the next section to derive a linearized set of equations.

Product of concentrations at equilibrium

For two different diffusing species at equilibrium, having concentrations c^{u} and c^{v} and valences z^{u} and z^{v}, the product $(c^{\mathrm{u}})^{1/z^{\mathrm{u}}}(c^{\mathrm{v}})^{-1/z^{\mathrm{v}}}$ is constant over space. To see this, consider the steady-state version of the flux equations given by

$$\boldsymbol{\nabla} c^{\mathrm{u}} - z^{\mathrm{u}} Q c^{\mathrm{u}} \boldsymbol{E} = \boldsymbol{0}, \tag{23}$$

$$\boldsymbol{\nabla} c^{\mathrm{v}} - z^{\mathrm{v}} Q c^{\mathrm{v}} \boldsymbol{E} = \boldsymbol{0}. \tag{24}$$

Dividing Eq. 23 by $z^{\mathrm{u}}c^{\mathrm{u}}$ and Eq. 24 by $z^{\mathrm{v}}c^{\mathrm{v}}$ and subtracting, we obtain

$$\frac{\boldsymbol{\nabla} c^{\mathrm{u}}}{z^{\mathrm{u}}c^{\mathrm{u}}} - \frac{\boldsymbol{\nabla} c^{\mathrm{v}}}{z^{\mathrm{v}}c^{\mathrm{v}}} = \boldsymbol{0} \Rightarrow \boldsymbol{\nabla} \ln((c^{\mathrm{u}})^{1/z^{\mathrm{u}}}(c^{\mathrm{v}})^{-1/z^{\mathrm{v}}}) = \boldsymbol{0},$$

from which it follows that

$$(c^{\mathrm{u}})^{1/z^{\mathrm{u}}}(c^{\mathrm{v}})^{-1/z^{\mathrm{v}}} = \text{const.} \tag{25}$$

For a salt solution with $z^{\mathrm{u}} = +1$ and $z^{\mathrm{v}} = -1$, this result says that the product $c^{+}c^{-}$ is constant at equilibrium. In dimensional variables, the constant is equal to unity; dimensionally, it is given by c_{blood}^2. Furthermore, from Eq. 25 it follows that at any two radial distances, r_1 and r_2,

$$c^{\mathrm{u}}(r_1)^{1/z^{\mathrm{u}}}c^{\mathrm{v}}(r_1)^{-1/z^{\mathrm{v}}} = c^{\mathrm{u}}(r_2)^{1/z^{\mathrm{u}}}c^{\mathrm{v}}(r_2)^{-1/z^{\mathrm{v}}},$$

from which we conclude

$$\left(\frac{c^{u}(r_1)}{c^{u}(r_2)}\right)^{1/z^{u}} = \left(\frac{c^{v}(r_1)}{c^{v}(r_2)}\right)^{1/z^{v}}. \quad (26)$$

This result becomes useful when solving for the equilibrium distribution of a species because it can be used to uncouple the zero-flux equations.

Implication for tracer exclusion in equilibrium

The results of the previous section have important implications for the exclusion of molecular tracers from regions where the glycocalyx fixed-charge density is large. To illustrate this, we initially restrict consideration to $z^+ = 1$ and $z^- = -1$. Subsequently, we will give an argument to generalize the results to arbitrary values of z^+ and z^-.

Using Eq. 26, and letting $r_1 = 0$, $r_2 = r$, $u = +$, and $v = L$ (so that $z^+ = 1$ and $z^L = -m$), we obtain

$$\frac{c^{L}(r)}{c^{L}(0)} = \left(\frac{c^{+}(r)}{c^{+}(0)}\right)^{-m}. \quad (27)$$

Similarly,

$$c^{+}(0)c^{-}(0) = c^{+}(r)c^{-}(r). \quad (28)$$

Recalling the definition of δ from Eq. 20, we note that $B \approx 4000$ in blood plasma, and also that nF is presumed to be large compared with m, which is $<\sim 5$ in the experiments of Vink and Duling (2000). Because all concentrations are nondimensional, they are of order unity so mc^L is negligible compared with the other terms. Also, because modest charge imbalances result in large forces, δ is generally assumed to be very small. Therefore,

$$z^{+}Bc^{+}(r) + z^{-}Bc^{-}(r) - nFc^{F}(r) \approx 0. \quad (29)$$

In the lumen, c^F is also negligible because the glycocalyx is assumed not to extend across the entire vessel (Vink and Duling, 1996, 2000). Since $c^F(0) = 0$, then at the center of the lumen $z^+c^+(0) \approx -z^-c^-(0)$. Using this in Eq. 28, and recalling the assumptions that $z^+ = +1$ and $z^- = -1$, Eq. 29 becomes

$$c^{+}(0)^2 \approx c^{+}(r)\left(c^{+}(r) - \frac{nF}{B}c^{F}(r)\right) \quad (30)$$

from which it follows that the nonnegative value of $c^+(r)$ is given by

$$\frac{c^{+}(r)}{c^{+}(0)} \approx \frac{1}{2}\left(\frac{nF}{B}\frac{c^{F}(r)}{c^{+}(0)} + \left(\left(\frac{nF}{B}\frac{c^{F}(r)}{c^{+}(0)}\right)^2 + 4\right)^{1/2}\right). \quad (31)$$

Now, for convenience we define

$$\xi(r) \equiv \frac{nF}{z^{+}B}\frac{c^{F}(r)}{c^{+}(0)} \quad (32)$$

and substitute Eq. 31 into Eq. 27 to obtain

$$\frac{c^{L}(r)}{c^{L}(0)} = \left(\tfrac{1}{2}\left[\xi(r) + (\xi(r)^2 + r)^{1/2}\right]\right)^{-m} \quad (33)$$

for $z^+ = -z^- = 1$. Because the concentrations are nondimensional, $c^+(0) = 1$, and if $r = r_0$ is chosen where the glycocalyx is most concentrated, then $c^F(r_0) = 1$. Thus, $\xi_0 = nF/(z^+B)$ measures the ratio of the glycocalyx fixed-charge density to the luminal concentration of free salts, and

$$\frac{c^{L}(r_0)}{c^{L}(0)} = \left(\tfrac{1}{2}\left[\xi_0 + (\xi_0^2 + r)^{1/2}\right]\right)^{-m}. \quad (34)$$

This quantity will be referred to as the exclusion factor because it gives the factor by which anionic molecular tracers are suppressed within the glycocalyx compared with the lumen. It is plotted against ξ_0 for several different values of m in Fig. 2. If ξ_0 and m are small, then $c^L(r_0)/c^L(0)$ approaches unity. If ξ_0 and m are large, then $c^L(r_0)/c^L(0)$ approaches zero, implying that the molecular tracers are excluded from the glycocalyx. Thus, if the fixed-charge density of the glycocalyx is large compared with the concentration of free salts in the blood, or if m is large, then anionic tracers are excluded from the glycocalyx. This plays a very important role in suppressing the flux of tracers through the glycocalyx, and thereby lengthening the diffusion time.

Equilibrium distribution for δ

The equilibrium configuration for δ can be determined from the zero-flux equation for c^+ corresponding to the dimensionless form of Eq. 14 given by

$$r\frac{dc^{+}}{dr} - z^{+}Qc^{+}\int_0^r \delta(\sigma)\sigma d\sigma = 0. \quad (35)$$

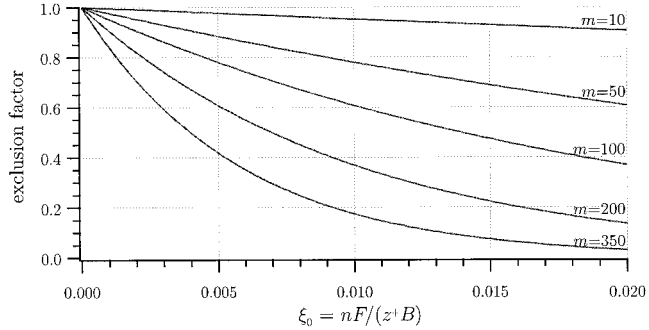

FIGURE 2 The dependence of the exclusion factor, Eq. 34, on ξ_0 for several different values of m.

We divide the zero-flux equation by c^+, which vanishes nowhere, and differentiate with respect to r to find

$$\frac{\mathrm{d}}{\mathrm{d}r}\left(r\frac{\mathrm{d}}{\mathrm{d}r}\ln(c^+)\right) - z^+Qr\delta = 0. \tag{36}$$

This immediately gives δ in terms of the distribution of c^+ such that

$$\delta(r) = \frac{1}{z^+Qr}\frac{\mathrm{d}}{\mathrm{d}r}\left(r\frac{\mathrm{d}}{\mathrm{d}r}\ln(c^+(r))\right). \tag{37}$$

Using Eq. 31, and recalling that $c^+(0) = 1$, we substitute for c^+ in Eq. 37 to obtain

$$\delta(r) = \frac{1}{z^+Qr}\frac{\mathrm{d}}{\mathrm{d}r}\left(r\frac{\mathrm{d}}{\mathrm{d}r}\ln\left(\frac{nF}{2B}c^{\mathrm{F}}(r) + \left(\left(\frac{nF}{2B}c^{\mathrm{F}}(r)\right)^2 + 1\right)^{1/2}\right)\right) \tag{38}$$

$$= \frac{1}{mQr}\frac{\mathrm{d}}{\mathrm{d}r}\left(r\frac{\mathrm{d}}{\mathrm{d}r}f(r)\right), \tag{39}$$

where

$$f(r) \equiv \frac{m}{z^+}\ln(c^+(r))$$

$$= \ln(\tfrac{1}{2}[\xi_0 c^{\mathrm{F}}(r) + ((\xi_0 c^{\mathrm{F}}(r))^2 + 4)^{1/2}])^{\mathrm{m}/z^+}. \tag{40}$$

Equation 38 shows that δ is related to the second derivative of the glycocalyx distribution, c^{F}. Since $Q = 72300$ for a typical capillary, δ is a small quantity, as assumed in the derivation of Eq. 29, making the assumption self-consistent. Based on dimensional considerations discussed earlier, this estimate for δ should be accurate to within one part in $z^+c_{\mathrm{blood}}/(mc_0^{\mathrm{L}}) = B/m \approx 1000$ even during the diffusion process. Next it will be shown that f is closely related to the voltage field induced in the neighborhood of the glycocalyx.

Induced voltage

Although electroneutrality has been imposed globally, concentration of the glycocalyx on the endothelial-cell wall gives rise to small departures from electroneutrality near the interface between the glycocalyx and the plasma in the lumen. The resulting electric field that arises from these charge imbalances can be calculated directly from δ using Eq. 8. Substituting the approximate analytic expression for δ, given by Eq. 39, into Eq. 8, and redimensionalizing, gives the electric field explicitly:

$$E_{\mathrm{r}} = \frac{kT}{mq}f'(r) = -V'(r). \tag{41}$$

The voltage is then given by:

$$V(r) = -\frac{kT}{mq}f(r) + V_0, \tag{42}$$

where V_0 is a constant of integration. Substituting for f in this expression from Eq. 40 gives

$$V(r) = -\frac{kT}{z^+q}\ln(\tfrac{1}{2}[\xi_0 c^{\mathrm{F}}(r) + ((\xi_0 c^{\mathrm{F}}(r))^2 + 4)^{1/2}]). \tag{43}$$

The reference voltage has been chosen to make the voltage zero within the lumen. This expression agrees with the interface potential quoted by Masaki et al. (2000).

LINEARIZED SOLUTION

In this section we invoke the approximation that $B/m \gg 1$ and use the results of the previous section to decouple and linearize the governing equations. This permits an eigenfunction solution to the problem. The value of the first nonzero eigenvalue, λ_1, is shown to have important implications for the diffusion time, and an asymptotic expression for λ_1 is found for a box-shaped distribution of the glycocalyx.

Quasi-static approximation for δ

The key observation is that although mc^{L} might significantly exceed δ throughout the system, δ varies only slightly as c^{L} changes with time. The physical justification for this is somewhat subtle. Before the addition of anionic molecular tracers, c^+ and c^- have been in the system sufficiently long to attain equilibrium with the glycocalyx molecules. This means that the electric field set up by the fixed charges bound to the glycocalyx is already supporting concentration gradients in $c^{\pm}$ near the glycocalyx. When tracers are added, they also diffuse through the glycocalyx; however, because $c_0^{\mathrm{L}} \ll c_{\mathrm{blood}}$ the presence of tracers introduces only a small perturbation to the free salt ion concentration. Thus, $c^{\pm}$ does not change significantly, and neither does the electric field, which continues to support concentration gradients in $c^{\pm}$. Therefore, δ is perturbed only slightly around its equilibrium value and remains nearly unchanged throughout the diffusion process. Essentially, the presence of anionic molecular tracers may only perturb δ by around one part in $B/m \approx 1000$.

This result can be derived formally by considering Eq. 37 in conjunction with the requirement of global charge balance. Because the additional cations must globally balance the charge on the anionic molecular tracers, we have

$$\int_0^1 z^+B(c^+(r, t) - c^+(r, t_0))r\mathrm{d}r = \int_0^1 mc^{\mathrm{L}}(r, t)r\mathrm{d}r \tag{44}$$

where $c^+(r, t_0)$ is the equilibrium distribution of cations before the tracers are added. Thus, the temporal variation of c^+ must be of order m/B, so we write $c^+(r, t_{\mathrm{f}}) = c^+(r, t_0) + (m/B)\Delta c^+(r)$, where $c^+(r, t_{\mathrm{f}})$ is the cation equilibrium distribution after the tracers have equilibrated, and $\Delta c^+(r)$ is of

order unity (in the sense that its volumetric integral on $0 \leq r \leq 1$ is unity). Substituting this expression into Eq. 37 gives

$$\delta(r, t_f) = \frac{1}{z^+ Qr}\frac{d}{dr}\left(r\frac{d}{dr}\ln(c^+(r, t_f))\right), \quad (45)$$

$$= \frac{1}{z^+ Qr}\frac{d}{dr}\left(r\frac{d}{dr}\ln\left[c^+(r, t_0) + \frac{m}{B}\Delta c^+(r)\right]\right), \quad (46)$$

$$= \delta(r, t_0) + \frac{m}{B}\frac{1}{z^+ Qr}\frac{d}{dr}\left(r\frac{d}{dr}\frac{\Delta c^+(r)}{c^+(r, t_f)}\right). \quad (47)$$

Thus, consistent with the qualitative arguments made previously, the fractional variation in δ is of order $m/B \approx 1/1000$, and is therefore negligible. Thus, δ can be considered quasi-static, and is well-approximated by the steady-state result given by Eq. 39.

Eigenvalue problem for static δ

Using the quasi-static approximation for δ in Eq. 39, the governing equations can be linearized and decoupled. Recalling Eq. 19, the conservation of mass for c^L is given by

$$D\frac{\partial c^L}{\partial t} = \frac{1}{r}\frac{\partial}{\partial r}\left(r\frac{\partial c^L}{\partial r} + mQc^L\int_0^r \delta(\sigma)\sigma\, d\sigma\right). \quad (48)$$

Substituting Eq. 39 for δ and integrating provide

$$D\frac{\partial c^L}{\partial t} \approx \frac{1}{r}\frac{\partial}{\partial r}\left(r\frac{\partial c^L}{\partial r} + r\frac{df}{dr}c^L\right). \quad (49)$$

This equation is linear in c^L and homogeneous, and is uncoupled from the conservation equations governing the other species. Separation of variables provides a series solution in terms of orthogonal functions. Thus, we seek multiplicatively separable solutions of the form $R(r)T(t)$ that satisfy Eq. 49 and the boundary conditions. Using standard methods (Boyce and DiPrima, 1992), a linear superposition of such solutions will provide an eigenfunction expansion that will be made to satisfy the initial condition at $t = t_0$. Substituting into Eq. 49 and separating r and t dependence we find

$$\frac{1}{rR}\frac{d}{dr}(rR' + rf'R) = D\frac{\dot{T}}{T} = -\lambda^2 \quad (50)$$

where λ is a real constant. In this form it is evident that $R(r)$ depends only on λ and $f(r)$, which in turn depend only on m, ξ_0, and $c^F(r)$. Because Eq. 49 is homogeneous, we conclude from the second of Eq. 50 that $T(t) = e^{-\lambda^2 t/D}$.

Because the flux must vanish at $r = 0$ and $r = 1$, according to Eqs. 12 and 13, the boundary conditions on $R(r)$ are simply $R'(0) = R'(1) = 0$. Imposing these boundary conditions provides a denumerable infinite set of eigenvalues, $\{\lambda_n\}_{n=0}^{\infty}$, corresponding to the set of eigenfunctions, $\{R_n(r)\}_{n=0}^{\infty}$, where each $R_n(r)$ must satisfy the ordinary differential equation (ODE) given by the first of Eq. 50. For $\lambda_0 = 0$, an analytic expression for $R_0(r)$ is found to within a multiplicative constant to be

$$R_0(r) = e^{-f(r)} = (\xi_0 c^F(r) + ((\xi_0 c^F(r))^2 + 4)^{1/2})^{-m}. \quad (51)$$

This corresponds to the equilibrium distribution for c^L after transients have decayed. To within a multiplicative constant factor, it is the same as Eq. 33. For the remaining eigenfunctions, $R_n(r)$, however, there is no analytic expression for general $f(r)$.

Orthogonality of $R_n(r)$

To obtain the eigenvalues and their associated eigenfunctions, the ODE given by the first of Eq. 50 must be solved numerically for R_n. An eigenfunction expansion, which is formed by the linear superposition of eigenfunctions, R_n, and which can be made to satisfy the initial condition, provides the series solution given by

$$c^L(r, t) = \sum_{n=0}^{\infty} c_n e^{-(\lambda_n^2/D)t}R_n(r). \quad (52)$$

The coefficients, c_n, are found by taking the inner product of the corresponding eigenfunction, $R_n(r)$, with the initial distribution, $c^L(r, t_0)$. The inner product is defined by a weight function, $w(r)$, with respect to which all of the eigenfunctions are orthogonal. If a linear ODE with variable coefficients can be written as a Sturm-Liouville boundary value problem with separated boundary conditions, one can show that the eigenfunctions of the ODE are orthogonal with respect to the weight function, $w(r)$ (Boyce and DiPrima, 1992). We therefore seek to transform the first of Eq. 50 into a Sturm-Liouville problem. The transformation must preserve the linearity of the ODE and should not add inhomogeneities to the boundary conditions. Thus we define $y(r) = R(r)/a(r)$, where $a(r)$ is to be determined. Substituting $y(r)$ into the left-hand side of Eq. 50 and equating coefficients with those of the Sturm-Liouville operator, it is easily shown that $a(r) = e^{-f(r)}$, and the ODE for y is then given by

$$ry'' + (1 - rf')y' = -\lambda^2 ry. \quad (53)$$

The eigenfunctions, $y_n(r)$, of the transformed problem are thus orthogonal with respect to the weight function $w(r) =$

$re^{-f(r)}$ so that

$$\frac{\int_0^1 y_m(r)y_n(r)re^{-f(r)}dr}{\int_0^1 y_n(r)^2re^{-f(r)}dr} = \frac{\int_0^1 R_m(r)R_n(r)re^{f(r)}dr}{\int_0^1 R_n(r)^2re^{f(r)}dr} = \begin{cases} 1 & \text{if } m = n \\ 0 & \text{if } m \neq n \end{cases}. \quad (54)$$

Because $f(r)$ is real and bounded, $w(r)$ is strictly positive. For a given initial concentration distribution, $c^L(r, t_0)$, of molecular tracers, the coefficients, c_n, are thus given by

$$c_n = \frac{\int_0^1 c^F(r, 0)R_n(r)re^{f(r)}dr}{\int_0^1 R_n(r)^2re^{f(r)}dr}. \quad (55)$$

Analytic solution for a box-shaped distribution in c^F

An analytic solution can be obtained if c^F has a box-shaped distribution of the form

$$c^F(r) = \begin{cases} 0 & \text{if } 0 \le r < r_g \\ 1 & \text{if } r_g \le r < r_{ec} \\ 0 & \text{if } r_{ec} \le r \le 1 \end{cases}.$$

This is the limiting case as $\Delta r_g \to 0$ and $\Delta r_{ec} \to 0$. For this distribution, f becomes (setting $z^+ = 1$ for simplicity)

$$f(r) = \begin{cases} 0 & \text{if } 0 \le r < r_g \\ \ln(\frac{1}{2}[\xi_0 + (\xi_0^2 + 4)^{1/2}])^m & \text{if } r_g \le r < r_{ec} \\ 0 & \text{if } r_{ec} \le r < 1 \end{cases}. \quad (56)$$

In this case, $f'(r)$ is just a linear combination of two Dirac delta functions given by

$$f'(r) = \ln(\tfrac{1}{2}[\xi_0 + (\xi_0^2 + 4)^{1/2}])^m \cdot (\hat{\delta}(r - r_g) - \hat{\delta}(r - r_{ec})). \quad (57)$$

Away from r_g and r_{ec}, $f'(r)$ is identically zero, so the ODE given by Eq. 53 becomes

$$ry'' + y' + \lambda^2 ry = 0, \quad (58)$$

the solution of which can be written as a piecewise linear combination of Bessel functions of the form

$$y(r) = \begin{cases} J_0(\lambda r) & \text{if } 0 \le r < r_g \\ \mathcal{A}J_0(\lambda r) + \mathcal{B}Y_0(\lambda r) & \text{if } r_g \le r < r_{ec} \\ \mathcal{C}J_0(\lambda r) + \mathcal{D}Y_0(\lambda r) & \text{if } r_{ec} \le r < 1 \end{cases}. \quad (59)$$

In the first interval, $0 \le r < r_g$, $Y_0(\lambda r)$ is omitted because it is unbounded as $r \to 0$, and the coefficient of $J_0(\lambda r)$ is taken as unity because the ODE is linear.

Near r_g and r_{ec}, a careful limiting process needs to be made to account for the Dirac delta function. The ODE given by Eq. 53 can be written as

$$\frac{y''}{y'} + \frac{(1 - rf')}{r} + \lambda^2\frac{y}{y'} = 0. \quad (60)$$

We first deal with the behavior near r_g. We assume that y' is nonzero around r_g (which will be checked for consistency below) and integrate over a small interval $(r_g - \epsilon, r_g + \epsilon)$ containing r_g to obtain

$$\ln(y')|_{r_g-\epsilon}^{r_g+\epsilon} + \ln(r)|_{r_g-\epsilon}^{r_g+\epsilon} - f|_{r_g-\epsilon}^{r_g+\epsilon} + \lambda^2\int_{r_g-\epsilon}^{r_g+\epsilon}\frac{y}{y'}dr = 0, \quad (61)$$

where $\epsilon > 0$. Because y' is assumed not to vanish on the interval, y/y' is bounded over the region of integration. Taking the limit as $\epsilon \to 0^+$ yields

$$\ln\left(\frac{y'(r_{g+})}{y'(r_{g-})}\right) - (f(r_{g+}) - f(r_{g-})) = 0. \quad (62)$$

Defining $\Delta f \equiv f(r_{g+}) - f(r_{g-})$ and using Eq. 56, we obtain

$$\Delta f = \ln(\tfrac{1}{2}[\xi_0 + (\xi_0^2 + 4)^{1/2}])^m. \quad (63)$$

Rearranging and taking the exponential of both sides of Eq. 62 yields

$$\frac{y'(r_{g+})}{y'(r_{g-})} = e^{\Delta f}. \quad (64)$$

This implies that as long as $y'(r_{g+}) \neq 0$ (an assumption made above), the first derivative is discontinuous at r_g, with $y'_+(r_g) = e^{\Delta f}y'_-(r_g)$. For nonzero Δf, the magnitude of the slope of y increases discontinuously at r_g. A similar result holds at r_{ec}, with Δf replaced by $-\Delta f$, so that $y'_+(r_{ec}) = e^{-\Delta f}y'_-(r_{ec})$.

Another condition on y is that its first derivative be bounded for all r; otherwise, an unphysical infinite flux would result. Therefore, y must be continuous at all points, and at r_g and r_{ec} in particular. It should be noted that this does not imply that R is continuous, as f is discontinuous for a box-shaped distribution.

The coefficients $\mathcal{A}$, $\mathcal{B}$, $\mathcal{C}$, and $\mathcal{D}$ are determined by the continuity requirement of y at r_g and at r_{ec}, the jump condition relating the first derivative of y at r_g and at r_{ec}, and the boundary condition, $y'(0) = y'(1) = 0$. In fact, the boundary condition at $r = 0$ is already met in the assumed form of the solution in Eq. 59, so only the boundary condition at $r = 1$ remains to be satisfied. These five constraints are expressed by the relations

$$J_0(\lambda r_g) = \mathcal{A}J_0(\lambda r_g) + \mathcal{B}Y_0(\lambda r_g), \quad (65)$$

$$J_1(\lambda r_g) = e^{-\Delta f}(\mathcal{A}J_1(\lambda r_g) + \mathcal{B}Y_1(\lambda r_g)), \quad (66)$$

$$\mathcal{A}J_0(\lambda r_{ec}) + \mathcal{B}Y_0(\lambda r_{ec}) = \mathcal{C}J_0(\lambda r_{ec}) + \mathcal{D}Y_0(\lambda r_{ec}), \quad (67)$$

$$\mathcal{A}J_1(\lambda r_{ec}) + \mathcal{B}Y_1(\lambda r_{ec}) = e^{\Delta f}(\mathcal{C}J_1(\lambda r_{ec}) + \mathcal{D}Y_1(\lambda r_{ec})), \quad (68)$$

$$\mathcal{C}J_1(\lambda) + \mathcal{D}Y_1(\lambda) = 0. \quad (69)$$

Throughout, the identities $J_0'(\lambda r) = -\lambda J_1(\lambda r)$ and $Y_0'(\lambda r) = -\lambda Y_1(\lambda r)$ have been used. There are five unknown parameters, $\mathcal{A}$, $\mathcal{B}$, $\mathcal{C}$, $\mathcal{D}$, and λ, and five equations, so there should be a solution as long as the equations are linearly independent. The equations are linear in $\mathcal{A}$, $\mathcal{B}$, $\mathcal{C}$, and $\mathcal{D}$, so any four of the five equations may be used to write the coefficients explicitly in terms of λ. The coefficients may be substituted into the remaining expression, resulting in a characteristic equation, denoted $\Upsilon(\lambda) = 0$, that involves λ as the only unknown. Coefficients $\mathcal{A}$ and $\mathcal{B}$ may be written in a fairly compact form; however, the expressions for $\mathcal{C}$, $\mathcal{D}$, and $\Upsilon(\lambda)$ are lengthy and are not explicitly shown here. They are, however, easily obtained using symbolic algebra software.

In any case, using numerical methods, the zeros of $\Upsilon(\lambda)$ can be found that determine the denumerable infinite set of eigenvalues, $\{\lambda_n\}_{n=0}^{\infty}$, that satisfy the constraints. A corresponding set of coefficients, $\{\mathcal{A}_n, \mathcal{B}_n, \mathcal{C}_n, \mathcal{D}_n\}_{n=0}^{\infty}$, can then be found by direct substitution of each λ_n into the characteristic equation, and then the eigensolutions for the box-shaped distribution are found. This solution requires the use of numerical techniques only to find the roots of an algebraic equation, so may be considered fully analytic.

Asymptotic approximation of λ_1 for monovalent mobile ions

Because the first nonzero eigenvalue, λ_1, determines the slowest transient in the solution, its value is a fundamental determinant of the electrochemical diffusion time scale. In particular, the dimensionless characteristic time scale associated with the first nonzero eigenvalue is given by $\tau_1 = D/\lambda_1^2$, and thus a long diffusion time is associated with a small value of λ_1. From the solution to the box-shaped distribution for c^F found above, it is possible to obtain a closed-form asymptotic approximation to λ_1 if either m is large or the fixed-charge density, nc_0^F, of the glycocalyx is large compared to the concentration of ions in the blood, i.e., if $\xi_0 \gg 1$ for $m > 0$. The characteristic equation for the eigenvalues of the box-shaped distribution, $\Upsilon(\lambda) = 0$, can be expanded in a Taylor series about $\lambda = 0$. It is known that Υ has a root at $\lambda = 0$, so the Taylor series is taken to $O(\lambda^5)$. The truncated Taylor expansion is cubic and has real roots at $\tilde{\lambda} = 0$ and $\pm\tilde{\lambda}_1$. If λ_1 is sufficiently small, the truncated Taylor series of the characteristic equation should be a good approximation to the original characteristic equation at least up to λ_1, that is, $\tilde{\lambda}_1 = \lambda_1 + O(\lambda^5)$. Although lengthy, $\tilde{\lambda}_1$ may be determined analytically. However, if we make the assumption that $M \equiv e^{\Delta f} \gg 1$, which is true if either m is large compared with unity, or nF is large compared with z^+B ($\xi_0 \gg 1$) and $m > 0$, we obtain a simple expression for $\tilde{\lambda}_1$. The Taylor expansion for $\tilde{\lambda}_1$ about $1/M = 0$ (i.e., about $M \to \infty$) is found to be

$$\lambda_1 \approx \tilde{\lambda}_1 = \left(\frac{2(1 - r_{ec}^2 + r_g^2)}{\ln(r_{ec}/r_g)(1 - r_{ec}^2)r_g^2}\right)^{1/2} \cdot M^{-1/2} + O(M^{-3/2}). \quad (70)$$

Recalling the definition of Δf and M, and discarding higher-order terms in $1/M$, we find the asymptotic solution for λ_1 as $\Delta f \to \infty$, for the box-shaped distribution of c^F, given by

$$\lambda_1 \approx \left(\frac{2(1 - r_{ec}^2 + r_g^2)}{\ln(r_{ec}/r_g)(1 - r_{ec}^2)r_g^2}\right)^{1/2} e^{-\Delta f/2}, \quad (71)$$

$$= \left(\frac{2(1 - r_{ec}^2 + r_g^2)}{\ln(r_{ec}/r_g)(1 - r_{ec}^2)r_g^2}\right)^{1/2} \cdot (\tfrac{1}{2}[\xi_0 + (\xi_0^2 + 4)^{1/2}])^{-m/2}. \quad (72)$$

This expression is extremely valuable for estimating λ_1. Comparison with numerically computed values of λ_1 reveals good agreement with the asymptotic form for $\lambda_1 < \sim 2$ (e.g., when $\xi_0 > \sim 10$ and $m = 1$, or when $\xi_0 > \sim 2$ and $m = 3$, or when $\xi_0 > \sim 0.06$ and $m = 100$). Although Eq. 72 was derived using the analytic solution for the box-shaped distribution, it does reveal the dependence of λ_1 on the parameters. The first factor on the right-hand side of Eq. 72 accounts for the geometry of c^F, while the second accounts for the role of F and m. Recalling the relationship between λ_1 and the characteristic diffusion time, τ_1, it is evident that

$$\tau_1 \propto D[\xi_0 + (\xi_0^2 + 4)^{1/2}]^m. \quad (73)$$

For $\xi_0 \gg 1$, $\tau_1 \propto D\xi_0^m$. This result illustrates the important influence of m and F on the electrochemical diffusion time of anionic molecular tracers. A more general asymptotic approximation of λ_1 for multivalent mobile ions is given in the Appendix.

NUMERICAL METHODS

The eigenvalue equation, given by Eq. 53, that arises from the linearized problem is solved numerically using a shooting method in conjunction with a commercial ODE solver (Mathematica). To validate the analysis of the previous section, numerical solutions of the coupled, nonlinear, partial, integro-differential equations in Eqs. 18 and 19 have also been obtained (with no asymptotic approximations) using a flux-conservative, Crank-Nicolson, finite-difference approach on an irregular grid. This numerical scheme handles the stiffness of the system and limits global error accumulation associated with the integral term. Details of the finite-difference methods used are discussed more fully in Stace (1999).

RESULTS

In this section, the results of the finite-difference solutions and analytical solutions are presented. The generality of the finite-difference scheme is shown to extend to cases where δ varies significantly with time. Through several tests, the scheme showed no numerical instabilities and achieved iteration convergence at each time step. Also, the accuracy of the static δ approximation is demonstrated when the assumptions of the derivation are met. Next, the results of the finite-difference and eigenvalue solutions are compared for a continuous glycocalyx distribution, establishing the validity of the latter for the case of static δ. Finally, the variation of the first nonzero eigenvalue with different glycocalyx distributions is explored. Unless otherwise stated, times given are nondimensional.

Finite difference scheme

When B/m or F/m is near unity, the static δ approximation is not valid. The finite-difference scheme is certainly capable of dealing with this situation, however. In Fig. 3, *a* and *b*, c^- is zero, so that c^+ just balances the charges on the glycocalyx and diffusing anionic molecules, making $B/m = 1$. Clearly, δ varies with time, decreasing in amplitude where the glycocalyx concentration varies most. When $B/m \gg 1$ or $F/m \gg 1$, the static δ approximation is seen to hold. For Fig. 3, *c* and *d*, $F/m = 285$ and $B/m = 800$. With this choice of parameters, temporal variation in δ is insignificant. In fact, near the glycocalyx boundary, δ changes by $<0.25\%$. The upper panels of Fig. 3 were initialized with a c^L distribution that followed a hyperbolic tangent distribution, while the lower panels were initialized with a Gaussian distribution of c^L. The diffusion times were found to be extremely insensitive to the initial c^L distribution.

The finite-difference scheme was checked for consistency using several methods. Most importantly, at each time step, the Newton-Raphson algorithm reduced the magnitude of the absolute residual of the coupled nonlinear difference equations to $<5 \times 10^{-8}$. Second, when $m = 0$, the coupled nonlinear equations are uncoupled and linear, and the resulting spatial eigenvalue problem may be written in terms of Bessel functions. Taking $m = 0$, the solutions obtained using this analytic method were compared with those obtained using the finite-difference approach on a nonuniform grid, and the relative pointwise difference between the two was $<1\%$ at each time step. Third, for nonzero m, the finite-difference code was run until variations were insignificant, and the resulting product of concentrations was seen to be constant over space, in agreement with Eq. 25. Finally, numerical solutions computed at two different (but small) time steps agreed within 0.5%.

Comparison between results of numerical solution and eigenfunction expansion

The eigenvalue problem formulated above is now compared, for a particular case, with the solution obtained using

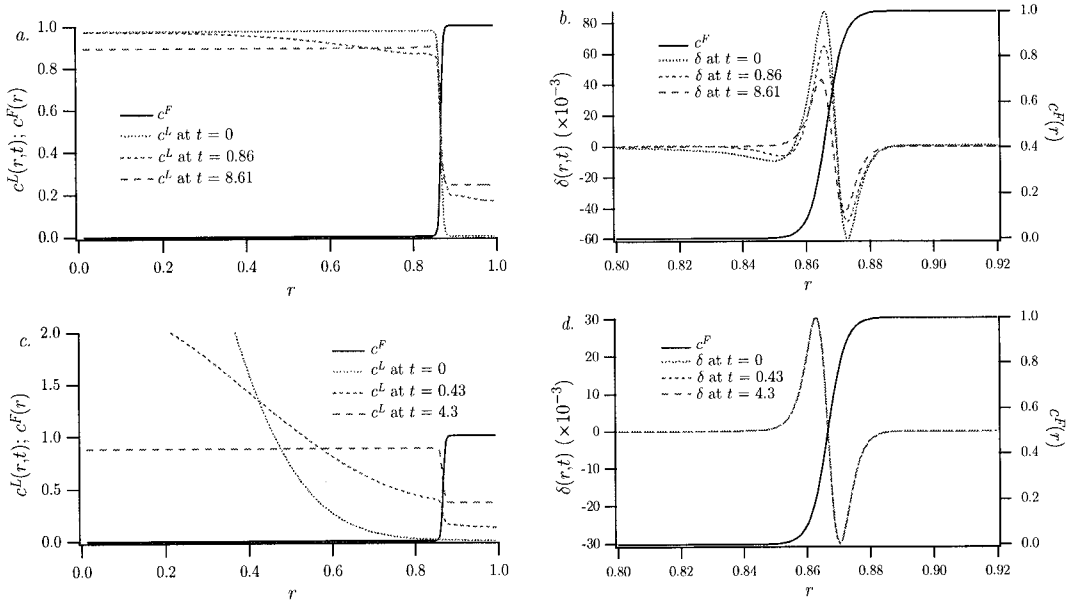

FIGURE 3 (*a*) Time variation of anionic molecular tracer concentration, $c^L(r, t)$, for $F/m = 1$ and $B/m = 1$. Note that the initial distribution for c^L follows a hyperbolic tangent. (*b*) Time variation of $\delta(r, t)$ corresponding to the instantaneous c^L distributions shown in (*a*). Note that δ varies significantly with time. (*c*) Time variation of anionic molecular tracer concentration for $F/m = 285$ and $B/m = 800$. In this case, the initial c^L distribution follows a Gaussian. (*d*) Time variation of $\delta(r, t)$ corresponding to the instantaneous c^L distributions shown in (*c*). Note that the instantaneous δ distributions are indistinguishable, which is consistent with a quasi-static approximation for δ. In all panels, $m = 5$, $Q = 72314$, and the geometric parameters are $r_g = 0.86$, $\Delta r_g = 0.02$, and $r_{ec} = 1$ such that there is no leakage into the extravascular space.

the finite-difference scheme. In the results shown in Fig. 3, the system boundary, where the flux of anionic tracers vanishes, was chosen as the endothelial-cell wall. All subsequent results account for leakage of tracers into the extravascular space. This is simulated by including a region past the endothelial-cell wall into which anionic molecular tracers can diffuse. Thus, for the results shown below, the c^F distribution is assumed to follow the form shown in Fig. 1, where $r_{ec} < 1$.

To find the eigenvalues, R_n is computed for different values of λ. The derivative, $R_n'(1; \lambda)$, evaluated at the system boundary, is plotted against λ and shown in Fig. 4 *a*. The eigenvalues correspond to the roots of the characteristic equation, $R_n'(1; \lambda) = 0$. In this case, the first three eigen-

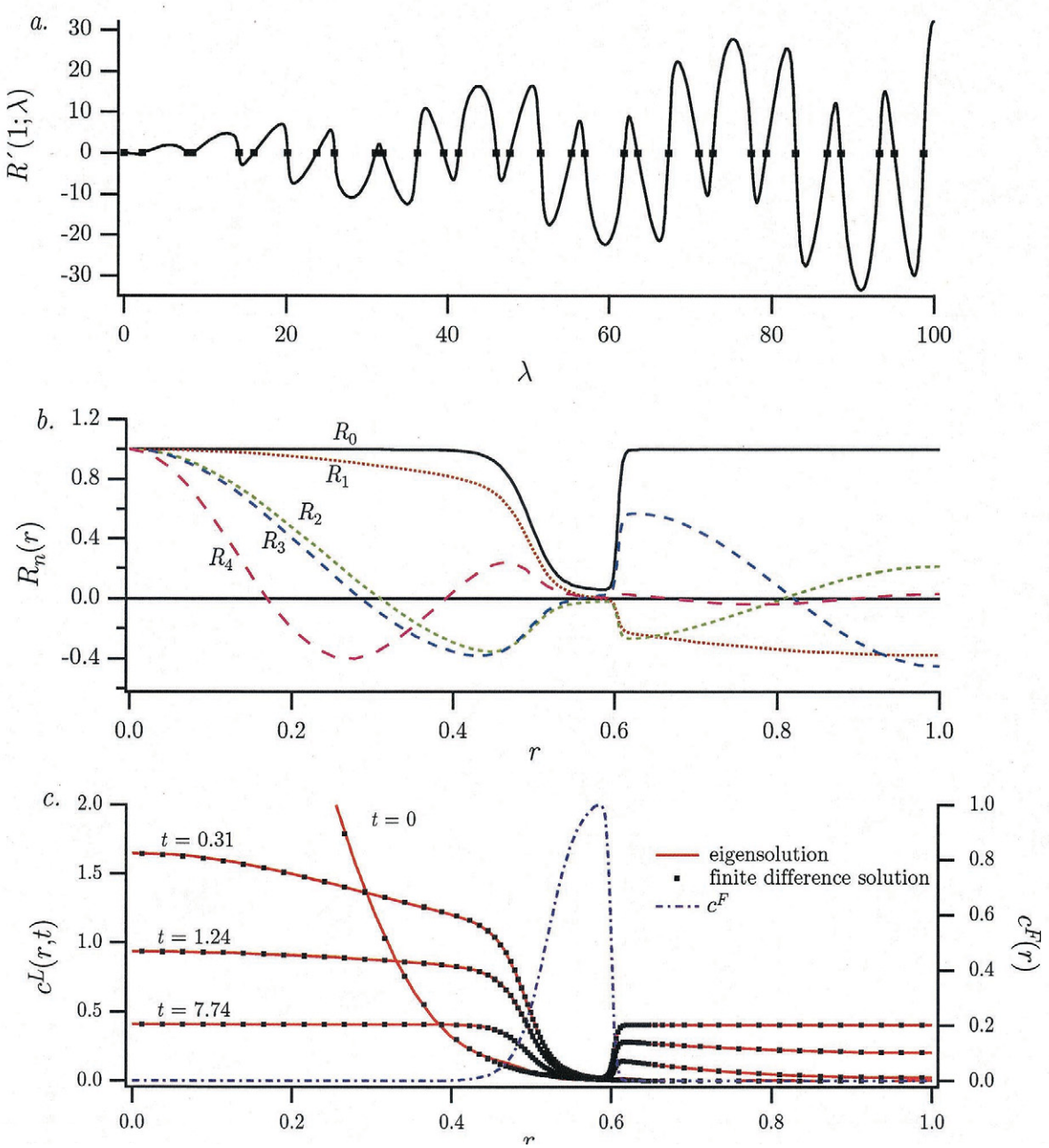

FIGURE 4 (*a*) Graphical representation of $R'(1; \lambda)$, corresponding to the left-hand side of the characteristic equation associated with the eigenvalue problem. As λ varies, so does $R'(1; \lambda)$. The eigenvalues, corresponding to the roots of the characteristic equation (*dots*), occur where $R'(1; \lambda)$ vanishes. (*b*) The first five eigenfunctions, $R_n(r)$. To within a constant multiplicative factor, the eigenfunction, $R_0(r)$, corresponds to the equilibrium distribution of c^L. (*c*) Comparison of the solutions obtained by the finite-difference method versus the eigenfunction expansion (truncated after the first 15 terms); c^F is also shown. For all panels, $F = 4744$, $B = 4000$, $Q = 200871$, $m = 5$, $r_g = 0.52$, $\Delta r_g = 0.2$, $r_{ec} = 0.6$, and $\Delta r_{ec} = 0.03$.

values are 0, 2.19, and 7.78. Each eigenvalue has a corresponding eigenfunction, and Fig. 4 *b* shows the first five eigenfunctions, $R_0, \ldots, R_4$, corresponding to $\lambda_0, \ldots, \lambda_4$.

For $F = 4744$, $B = 4000$, and $m = 5$, the instantaneous distributions of c^L, computed from the eigenfunction expansion truncated after 15 terms, are shown in Fig. 4 *c* at various times. Also shown are the corresponding results found using the finite-difference scheme. The agreement between the two methods is excellent, differing most (although not apparent from the figure) where c^F is large.

Time variation of c^L for box-shaped distribution

For $F = 235200$, $B = 4000$, and $m = 3$, Fig. 5 shows the distribution of c^L computed for a box-shaped distribution using the first 10 terms of the fully analytic eigenfunction expansion derived previously. The diffusion process has two characteristic time scales. In a short time, c^L reaches pseudo-equilibrium, with imperceptible concentration gradients over each region. For the parameters used in the results shown in Fig. 5, it takes $\sim 10^5$ times longer for the anionic molecules to leak through the glycocalyx and establish equilibrium. This illustrates the stiffness of this problem, as mentioned in the previous section. Note also that the shape of the concentration distribution for $r < r_g$ (where c^F is negligible) is very similar to what would be expected for diffusion driven solely by chemical potential gradients.

Variation of λ_1

While $\lambda_0 = 0$ is associated with the equilibrium configuration, the nonzero eigenvalues, λ_n, are associated with the transient dynamics, and are related to the nondimensional characteristic diffusion times according to $\tau_n = D/\lambda_n^2$. Because transients corresponding to λ_n decay faster with increasing n, the slowest time constant is associated with the first nonzero eigenvalue, λ_1. Whereas τ_1 depends on the dimensionless diffusion coefficient ratio, D, λ_1 does not, and results are therefore more generally expressed in terms of the latter. As λ_1 depends on f, it varies with m, $\xi_0 = nF/(z^+B)$, and the geometric parameters r_g, r_{ec}, Δr_g, and Δr_{ec} appearing in Eq. 22. In what follows, the dependence of λ_1 on these parameters will be examined.

Dependence on ξ_0

The variation of λ_1 with ξ_0 is shown in Fig. 6 for several values of the valence magnitude, m. Since ξ_0 represents the glycocalyx fixed-charge density relative to the valence-weighted concentration of ions in the blood, Fig. 6 reveals the influence of the fixed charges on the diffusion time. The solid curves correspond to a smoothly varying c^F distribution, for which $r_g = 0.4$, $\Delta r_g = 0.1$, $r_{ec} = 0.5$, and $\Delta r_{ec} = 0.03$. For all positive values of m, as $\xi_0 \to 0$ (i.e., as the exclusion factor approaches unity), λ_1 asymptotes to 3.8317 for the solid and dotted curves. This is precisely the first nonzero root of $J_1(r) = 0$, which corresponds to the first nonzero eigenvalue if diffusion were driven by chemical gradients alone. As $\xi_0 \to \infty$, λ_1 decreases monotonically for all values of m according to the power-law relationship, $\lambda_1 \propto \xi_0^{-\vartheta}$, where ϑ, which depends upon m, is the slope of the log-log plot shown in Fig. 6. Results for the box-shaped distribution, corresponding to the dotted curves in Fig. 6, show that λ_1 is consistently lower than for the smooth

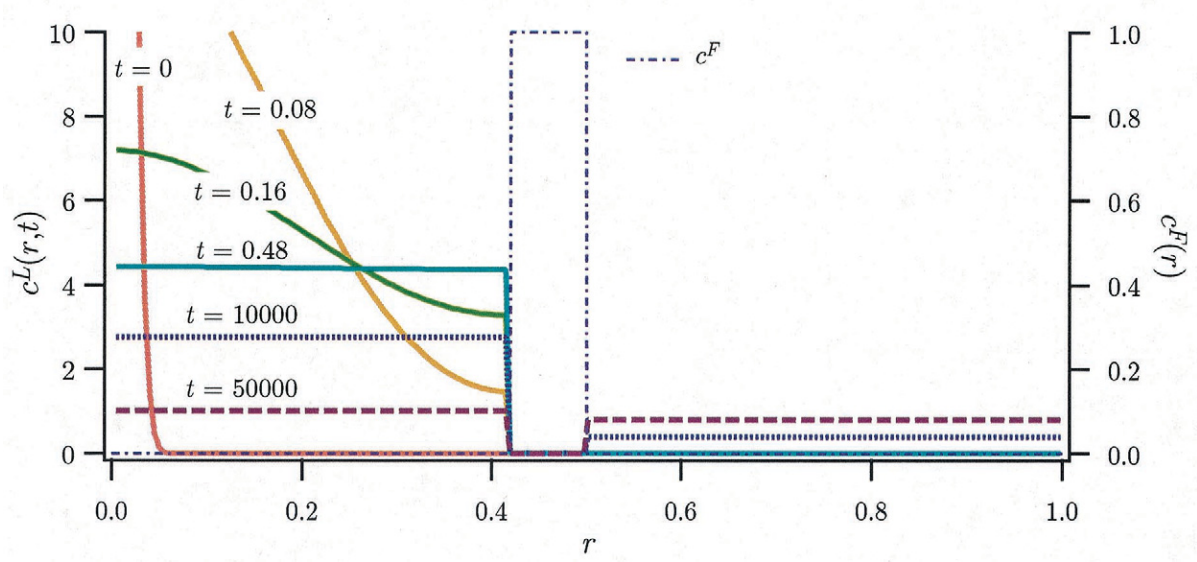

FIGURE 5 Plots of $c^L(r, t)$ at various times assuming a box-shaped distribution for c^F with $F = 235{,}200$, $B = 4000$, and $m = 3$. The c^F distribution is shown (*dot-dash*) as the rectangle extending from $r_g = 0.42$ to $r_{ec} = 0.5$.

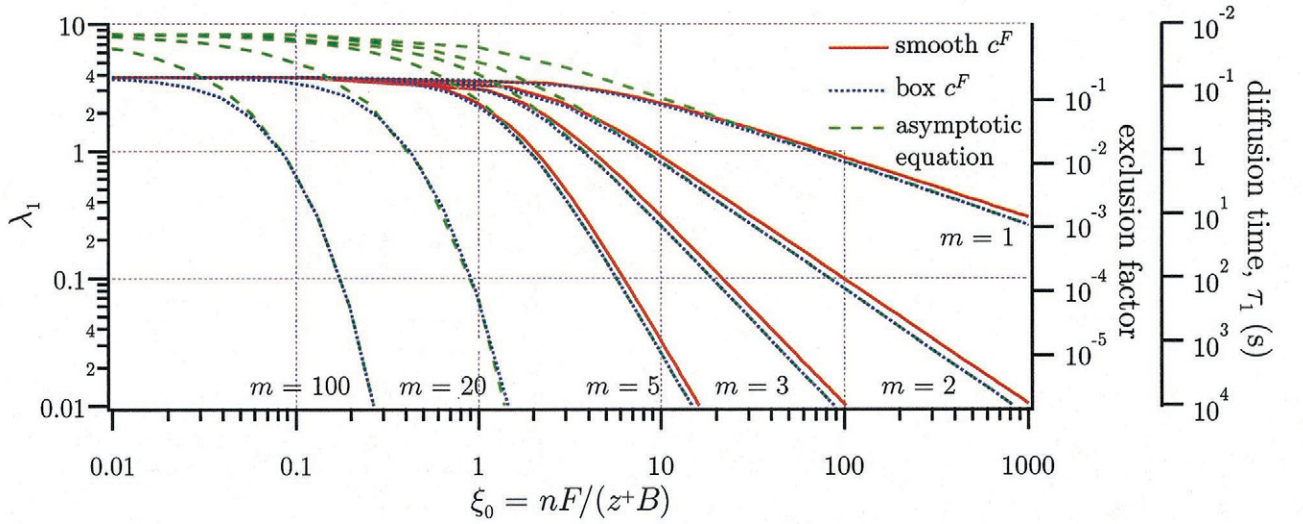

FIGURE 6 Dependence of λ_1 on ξ_0 for different values of anionic molecular valence magnitude, m. The solid lines correspond to λ_1 found by numerically solving the eigenvalue problem for $r_g = 0.4$, $\Delta r_g = 0.1$, $r_{ec} = 0.5$, and $\Delta r_{ec} = 0.03$. The dashed lines are the results for the corresponding box-shaped distribution, and the dotted lines show the asymptotic approximation of λ_1 for the box-shaped distribution. Agreement for the last two is excellent for $\lambda_1 < 2$. It should be noted that the asymptotic approximations in all cases converge to $\lambda_1 = 8.244$ as $\xi_0 \to 0$, whereas the correct limit is $\lambda_1 = 3.8317$, as can be seen from the solutions to the eigenvalue problem. Thus the asymptotic formula given by Eq. 72 is not valid for $\lambda_1 > \sim 2$. The two right-hand axes show the exclusion factor given by Eq. 34 and the diffusion time, τ_1, given by Eq. 74. Whereas λ_1 and the exclusion factor are independent of either the diffusion coefficient or the geometric parameters of the system, τ_1 depends on both. In computing τ_1, the diffusion coefficient, D^L, was taken to be 2.4×10^{-11} m^2/s and the system radius, $\mathcal{R}$, was taken to be 5 μm.

distribution, indicating that the gradients in c^F do have some effect on λ_1. The solution for the box-shaped distribution does capture the important trends in λ_1, however, and differs from the smooth distribution for the cases shown by $< \sim 15\%$ for $\lambda_1 < \sim 2$. The dashed curves show the variation in λ_1 calculated using the asymptotic approximation given by Eq. 72. The box-shaped distribution clearly converges to the asymptotic expression as $\xi_0 \to \infty$, which gives a very good approximation to λ_1 for the box-shaped distribution when $\lambda_1 < \sim 2$. The asymptotic formula given by Eq. 72 indicates that the slope of the log-log plot should be $\vartheta = -m/2$, which is clearly seen for each of the sets of curves in Fig. 6.

Dependence on *m*

The solid curves in Fig. 7 show how λ_1 varies with m for a smoothly varying c^F distribution taking geometric parameters $r_g = 0.4$, $\Delta r_g = 0.1$, $r_{ec} = 0.5$, and $\Delta r_{ec} = 0.03$. The value of λ_1 is calculated for values of m ranging from 0 to 6. Although noninteger values of the valence magnitude, m, may seem unphysical, due to charge shielding, the effective valence of anionic molecular tracers is typically not integer-valued. Results clearly show a strong dependence on m. In particular, for $m > 1$ it appears that this dependence has an exponential character of the form $\lambda_1 \approx \theta^{-m}$, where θ, which depends upon ξ_0, is the slope of the log-linear plot shown in Fig. 7. The dotted curves are calculated for the box-shaped distribution, and the dashed curves correspond to the asymptotic approximation for λ_1 given by Eq. 72. Agreement between the asymptotic expression and the eigenfunction expansion is good for $\lambda_1 < \sim 2$. The exponential relationship between λ_1 and m is predicted by Eq. 72, which indicates that for large ξ_0, λ_1 is proportional to $\xi_0^{-m/2}$. For a log-linear plot of λ_1 versus m, the slope of this relation will be $\theta = 1/2 \ln(\xi_0)$. The asymptotic slope of the log-linear curve corresponding to $\xi_0 = 119$ is predicted to be $\theta = 1.04$, which is in good agreement with the results shown in Fig. 7. Also of note is that as $m \to 0$, $\lambda_1 \to 3.8317$ for the solid and dotted curves at all values of ξ_0. Thus, the eigenvalue problem certainly reduces to that of Bessel's equation as $m \to 0$.

Dependence on system geometry

The geometry of the axisymmetric model is determined by the parameters r_g, Δr_g, r_{ec}, and Δr_{ec}. Varying r_{ec} while holding all other parameters constant corresponds to varying the radius of the extravascular cavity relative to the luminal radius. Fig. 8 *a* shows the relationship between λ_1 and r_{ec} for $\xi_0 = 11.9$ and $m = 5$. The value of r_{ec} was varied from 0.02 to 1, while the dimensions of the glycocalyx were kept constant relative to r_{ec}. In particular, $r_g = 0.75\ r_{ec}$, $\Delta r_g = 0.5\ r_{ec}$, and $\Delta r_{ec} = 0.05\ r_{ec}$. An important feature to note is that λ_1 is inversely proportional to r_{ec} (indicated by the -1 slope in the log-log plot), if $c^F(r)$ is small near $r =$

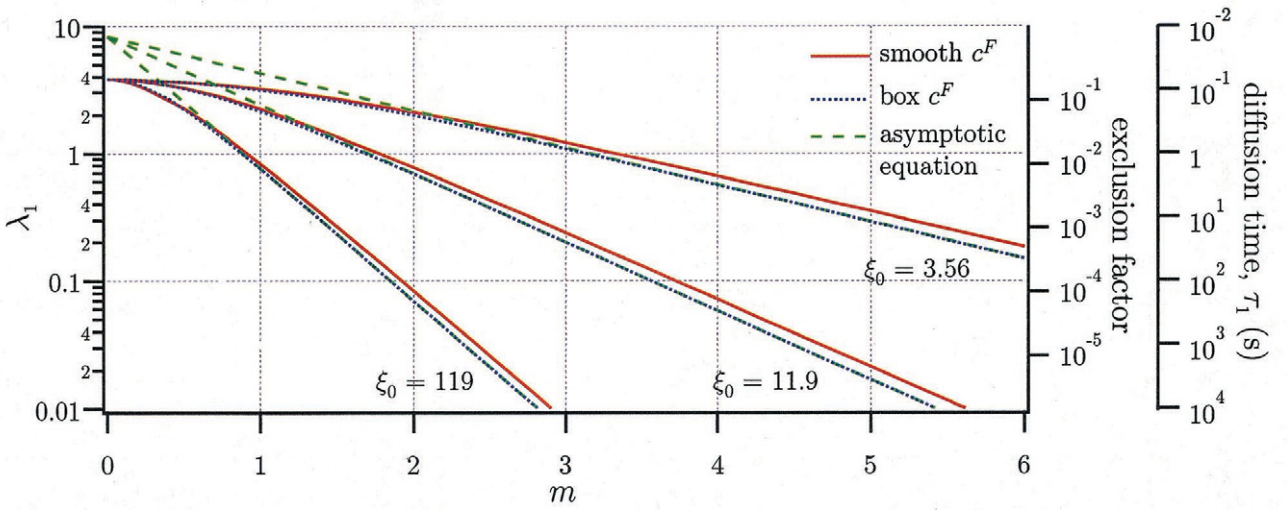

FIGURE 7 Dependence of λ_1 on the valence magnitude, m, of the anionic molecular tracer for different values of ξ_0. The solid lines correspond to λ_1 found by numerically solving the eigenvalue problem for a smoothly varying c^F distribution with $r_g = 0.4$, $\Delta r_g = 0.1$, $r_{ec} = 0.5$, and $\Delta r_{ec} = 0.03$. The dotted lines are the results for the corresponding box-shaped distribution and the dashed lines show the asymptotic approximation of λ_1 for the box-shaped distribution. Agreement is excellent for $\lambda_1 < 2$. The linearity of the results on the log-linear plot illustrates well the exponential dependence of λ_1 on the valence magnitude, m, for $\lambda_1 < 2$. It should be noted that, as in Fig. 6, the asymptotic approximations in all cases converge to $\lambda_1 = 8.244$ as $\xi_0 \to 0$, whereas the correct limit is $\lambda_1 = 3.8317$. The two right-hand axes show the exclusion factor given by Eq. 34 and the diffusion time, τ_1, given by Eq. 74. In computing τ_1, the parameters used were the same as in Fig. 6.

1. As can be seen from Eq. 72, this arises because all geometric terms in Fig. 8 *a* are proportional to r_{ec}. When $r_{ec} \approx 1$, the boundary of the system is near the capillary wall, resulting in very little leakage into the extravascular space. In this case, λ_1 jumps sharply to ~6.7 for the smooth c^F, and becomes infinitely large for the box-shaped distribution. Both reveal the same qualitative dependence on r_{ec}, with λ_1 for the box-shaped distribution being ~50% of its value for the smooth distribution at a given value of r_{ec}.

Varying r_g while holding all other parameters constant corresponds to changing the thickness of the glycocalyx relative to the luminal space. Fig. 8 *b* shows the variation of λ_1 with r_g for $\xi_0 = 11.9$, and $m = 5$. The value of r_g was varied between 0.1 and 0.595 while all other dimensions of the glycocalyx were kept constant relative to r_g. In particular, $\Delta r_g = 0.1$, $r_{ec} = 0.6$, and $\Delta r_{ec} = 0.03$. The solid curve, corresponding to the smoothly varying c^F, shows a qualitatively different behavior as r_g approaches r_{ec}. This arises due to the fact that, when $r_{ec} - r_g < \Delta r_g/2 = 0.05$, the general form of the c^F distribution near the endothelial-cell wall transitions from having a very sharp peak to having a rather flat distribution.

Varying Δr_g or Δr_{ec} changes the range over which c^F increases or decreases near r_g or r_{ec}, respectively. Results showed that λ_1 is relatively insensitive to both of these parameters. For one computation, parameters were fixed at

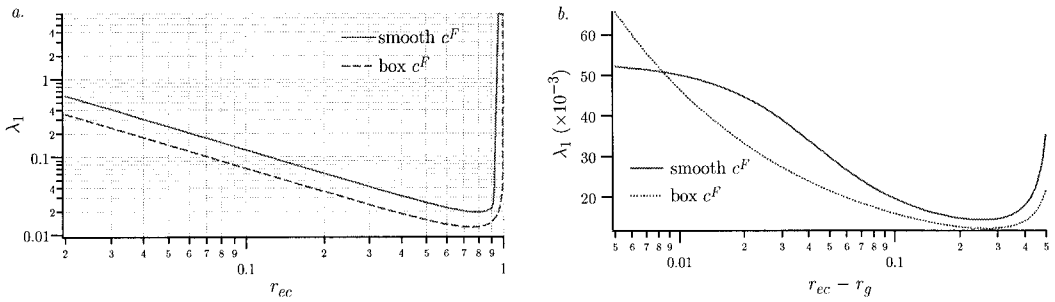

FIGURE 8 (*a*) Dependence of λ_1 on r_{ec} for $\xi_0 = 11.9$ and $m = 5$. The geometric parameters are fixed relative to r_{ec} such that $r_g = 0.75\ r_{ec}$, $\Delta r_g = 0.5\ r_{ec} = 0.03$, and $\Delta r_{ec} = 0.5\ r_{ec}$. This result may be interpreted as the variation of λ_1 with changing cavity size, but fixed capillary diameter and glycocalyx shape. The solid curve is calculated for a smoothly varying c^F, while the dashed curve is the corresponding solution for the box-shaped distribution. (*b*) Dependence of λ_1 on r_g for a smooth distribution of c^F (*solid curve*), and for the box-shaped distribution (*dotted curve*). Other parameters are fixed at $\xi_0 = 11.9$, $m = 5$, $r_{ec} = 0.6$, and $\Delta r_{ec} = 0.03$. The unusual behavior of the solid curve for small $r_{ec} - r_g$ occurs because the value of Δr_g is large enough relative to $r_{ec} - r_g$ to cause the distribution to be sharply peaked, rather than flat near the endothelial-cell wall.

$\xi_0 = 11.9$, $m = 5$, $r_g = 0.45$, and $r_{ec} = 0.6$. Setting $\Delta r_{ec} = 0.03$, and varying Δr_g by a factor of 10, from 0.05 to 0.5, the computed value of λ_1 showed an approximately twofold variation, increasing nearly linearly from 0.015 to 0.03. For these same parameters, the corresponding solution for the box-shaped distribution, which is independent of Δr_g and Δr_{ec}, is $\lambda_1 \sim 0.014$. This value corresponds to the limit for the solution to the smooth distribution as $\Delta r_g \to 0$. It was found that λ_1 was even less sensitive to the value of Δr_{ec} than it was to Δr_g. Setting $\Delta r_g = 0.2$, and varying Δr_{ec} by a factor of 20, from 0.02 to 0.4, the computed value of λ_1 varied only by ~18%, increasing nearly linearly from ~0.017 to 0.02.

DISCUSSION

Figs. 4 *c* and 5 reveal the transient electrochemical dynamics of anionic molecular transport through the layer. Owing to the solid-bound fixed charges on the glycocalyx, the model predicts that negative ions in the blood and diffusing anionic molecular tracers are partially excluded from the glycocalyx in equilibrium. These concentration gradients are supported by the electric field that is set up by the negative charges bound to the glycocalyx. A gradient-induced diffusion of anionic molecules from the capillary lumen into the glycocalyx is then limited by this electrostatic exclusion. If leakage of anionic molecules out of the capillary occurs, the concentration gradient begins to decrease between the lumen and the glycocalyx and increase between the glycocalyx and extravascular space. Because the levels of anionic molecular tracers remain suppressed within the glycocalyx throughout the diffusion process, tracers are passively transported against a concentration gradient as they diffuse into the extravascular space. These electrochemical dynamics drive the system to a new equilibrium state. Results indicate that a significant departure from Fickian diffusion occurs particularly if the valence magnitude of the diffusing anionic molecule is large and/or the fixed-charge density of the glycocalyx is large compared with the concentration of ions in the blood.

The close agreement between the results of the finite-difference solution and the eigenfunction expansion lends strong support to the accuracy of both in solving the governing equations, as long as the approximations $B/m \gg 1$ and $nF/m \gg 1$ are met. The eigenfunction expansion is much easier to implement and is much faster computationally. As long as the charge concentration of molecular tracers is small compared to the ion concentration in blood and to nc_0^F, it is much simpler to discuss the diffusion time in terms of the solution to the eigenvalues of the linear problem. However, even if B/m and nF/m are not large compared with unity, such that the quasi-static approximation for δ may not be valid, the finite-difference solution can still be used to examine the electrochemical transport of anionic molecular tracers through the layer.

Asymptotic diffusion time

The most important result of the previous section is that, for large m or $\xi_0 \gg 1$, λ_1 is much smaller than its value of ~3.8317 for $\xi_0 = m = 0$, when only chemical diffusion exists. Figs. 6 and 7 clearly show reductions of two orders of magnitude in λ_1 for moderate values of m. Recalling the relationship, $\tau_1^* = D/\lambda_1^2$, between the dimensionless characteristic diffusion time, τ_1^*, and λ_1, it is obvious that a two-order-of-magnitude reduction in λ_1 leads to an increase in the diffusion time of four orders of magnitude. The reduction of λ_1 by such an enormous amount rests on two requirements examined throughout the development of the previous sections. First, it requires the presence of a fixed, anionically charged glycocalyx, so that $nF \neq 0$ with either m is large or $\xi_0 \gg 1$. Second, tracers need to leak from the lumen into extravascular space, or the system will equilibrate in about one (Fickian) characteristic time constant. If either requirement is not met, then the governing equations will not predict the prolonged diffusion times observed by Vink and Duling (2000).

The physical reason for the reduction in λ_1 is not immediately obvious. Essentially, the near balance between the chemical and electrostatic potentials causes the anionic molecular tracers to be excluded from the glycocalyx; this, in turn, causes a retardation in transport through the layer because the flux scales according to the reduction in tracer concentration in the layer. The presence of free salt ions is important, as these set up the electrostatic potential against which the anionic tracers must move.

From the asymptotic formula for λ_1, given by Eq. 72, we obtain an expression for the dimensional diffusion time of molecular tracers given by

$$\tau_1 \approx \frac{r_g^2}{2D^L} \ln\left(\frac{r_{ec}}{r_g}\right)\left(\frac{\mathcal{R}^2 - r_{ec}^2}{\mathcal{R}^2 - r_{ec}^2 + r_g^2}\right) \cdot (\tfrac{1}{2}[\xi_0 + (\xi_0^2 + 4)^{1/2}])^m. \tag{74}$$

In the previous section, it was noted that the dimensional diffusion time is nearly independent of the system radius, $\mathcal{R}$, when the extravascular space is large compared to the capillary. This follows from Eq. 74, where it may be seen that if $\mathcal{R} \gg r_{ec} > r_g$, then the third factor on the right-hand side is nearly unity, and the diffusion time becomes independent of $\mathcal{R}$. Invoking this approximation, Eq. 74 reduces to

$$\tau_1 \approx \frac{r_g^2}{2D^L} \ln\left(\frac{r_{ec}}{r_g}\right)(\tfrac{1}{2}[\xi_0 + (\xi_0^2 + 4)^{1/2}])m. \tag{75}$$

This approximate form of the diffusion time differs from the exact value by <10% when $r_{ec} = 0.3\ \mathcal{R}$, which seems reasonable for microvascular networks of mammalian skeletal muscle as long as the capillary density is low enough to allow a mean center-to-center intercapillary separation of ~20 μm or more.

Some physically significant insights into the diffusion time can be had from Eq. 75. The first factor in the product on the right-hand side of Eq. 75 is one-half of a characteristic transit time, from the center of the capillary to the glycocalyx interface. The geometric factors in the middle reveal the dependence of the diffusion time on the thickness of the glycocalyx. In particular, because r_{ec}/r_g is near unity, the diffusion time scales approximately linearly with glycocalyx thickness. The last factor in the product represents the ratio of the molecular tracer concentration in the blood to that in the glycocalyx, as can be seen by comparison to Eq. 33. Thus, the diffusion time, which increases exponentially with the magnitude of the tracer valence, varies in inverse proportion to the anionic molecular exclusion factor.

Parameter values

On the basis of erythrocyte and macromolecular exclusion zones observed by Vink and Duling (1996, 2000), we assume the in vivo thickness of the glycocalyx to be $\sim$0.4 μm. The other geometric parameters used in the model depend upon capillary diameter and capillary density in the tissue and are given in Table 1. As we have seen, however, predicted diffusion times depend weakly on the geometric parameters.

The luminal concentration of Na^+ and Cl^- ions in blood is known to be $\sim$0.14 mol/l, and the luminal concentration of the molecular tracer is $\sim 3.5 \times 10^{-5}$ mol/l for 39 kDa FITC-dextran tracers, but varies with molecular weight. Because it is thought that the glycocalyx is extremely diffuse, it will be assumed that the diffusion coefficients, $D^{\pm}$, associated with the mobile ions, and D^L, associated with the smaller molecular tracers used by Vink and Duling (2000), are nearly the same in the glycocalyx as they are in water. Furthermore, for tracers $<$39 kDa, the diffusion coefficient is assumed to vary with the square root of the molecular weight of the diffusing species. For Na^+, the diffusion coefficient, D^+, in water is known to be $\sim 10^{-9}$ m^2/s. The diffusion coefficient, D^L, is then estimated by reducing D^+ by the square root of the relative molecular weights of Na^+ and the molecular tracer. This estimate yields values consistent with those estimated from intravital microscopy measurements of interstitial FITC-dextran concentrations (Fox and Wayland, 1979; Ley and Arfors, 1986). For example, for a 39-kDa FITC-dextran tracer, $D^L \approx (\mathrm{MW}(Na^+)/\mathrm{MW}(\mathrm{tracer}))^{1/2} D^+ \approx 2.4 \times 10^{-11}$ m^2/s. Because interstitial and free diffusion coefficients are reported to differ only by about a factor of four for 3-kDa FITC-dextran tracers (Ley and Arfors, 1986), we assume D^L to be constant throughout the system, including the extravascular space. It seems likely, however, that for dextran tracers $>$40 kDa, the glycocalyx and interstitium offer increasing steric hindrance with increasing molecular weight, and completely exclude dextrans larger than 70 kDa (Vink and Duling, 1996, 2000). The applicability of the model, therefore, to dextran tracers in excess of 40 kDa is uncertain because the idealized model of Brownian motion through the glycocalyx is not likely to be valid. Furthermore, no account is taken of macromolecular reflection in the extravascular space, and because the reflection coefficients become appreciable for FITC-dextran molecules in excess of 40 kDa (Curry, 1984), we limit attention to the smaller tracers used in the experiments of Vink and Duling (2000).

The most significant uncertainty in all of the parameters used in the model lies in our estimation of the magnitude, m, of the molecular tracer valence. In the experiments of Vink and Duling (2000), anionic fluorescent tracers are conjugated to macromolecules, such as dextran, so the valence of the conjugated molecular tracers is determined by the number of tracers that bind to the macromolecule. There may be some variation in this number, making the valence uncertain. Also, because some of the molecular tracer conjugates are very large molecules, some charge shielding may take place, making the valence magnitude, m, nonintegral. The range of m, corresponding to the valence magnitude associated with each of the anionic FITC-dextran conjugates, is listed in Table 2 in order of increasing molecular weight (Molecular Probes Inc., Eugene, OR).

Comparison with experimental findings

For the diffusion experiments reported by Vink and Duling (2000), 4-, 17-, and 39-kDa FITC-dextran molecules were used. The corresponding half lives, $\tau_{1/2}$, were reported to be 12, 22, and 90 min, respectively (Vink and Duling, 2000). The diffusion time, τ_1, of Eq. 75 is the 1/e diffusion time, which is related to the half-life by $\tau_1 = \ln(2)\, \tau_{1/2}$. Using the parameter values listed in Table 1 and the diffusion half-lives reported by Vink and Duling (2000), the value of $\xi_0 = nF/B = nc_0^F/c_{blood}$ can be inferred from Eq. 75. For each

TABLE 2 Range of ξ_0 predicted by Eq. 75 that is necessary to account for the prolonged dextran diffusion times ($\tau_{1/2}$) reported by Vink and Duling (2000)

MW	D^L (m^2/s)	$\tau_{1/2}$ (s)	τ_1 (s)	Valence Magnitude, m	Fixed-Charge Density
4	7.6×10^{-11}	720	504	$0.5 \le m \le 2$	$290 \le \xi_0 \le 7.4 \times 10^9$
17	3.7×10^{-11}	1320	924	$1 \le m \le 2$	$270 \le \xi_0 \le 7.7 \times 10^4$
39	2.4×10^{-11}	5400	3780	$3 \le m \le 7$	$5.5 \le \xi_0 \le 58.8$

Each range of ξ_0 shown corresponds to the given range of m associated with each of the three dextran tracers listed (Molecular Probes Inc., Eugene, OR). The geometric parameters were chosen such that $r_g = 2$ μm and $r_{ec} = 2.5$ μm (Vink and Duling, 1996, 2000).

dextran fraction used in the experiment, the range of ξ_0 corresponding to the range of m is presented in Table 2.

It is evident from Table 2 that there is no single value of ξ_0 that provides a consistent explanation for all of the diffusion times reported by Vink and Duling (2000). In fact, the ranges for ξ_0 corresponding to the two smaller dextran tracers do not overlap with the range corresponding to the 39-kDa tracer. Furthermore, considering the fixed-charge density of other mucopolysaccharide gels, the smallest value of ξ_0 that is able to reproduce the prolonged diffusion times reported by Vink and Duling (2000) for the smaller two tracers listed in Table 2 is several orders of magnitude larger than physiologically plausible. For example, the fixed-charge density of the tectorial membrane in the cochlea is reported to be $\sim$0.02 Eq/l on the basis of its composition. A recent estimate based on direct voltage measurements of the membrane places the estimate closer to 0.15 Eq/l (Masaki et al., 2000). An upper bound on the fixed-charge density of articular cartilage is reported as being $\sim$0.18 Eq/l (Maroudas, 1975). However, the presence of collagen in cartilage constrains the expansion of the proteoglycan and GAG aggregates, which results in a swelling pressure in the matrix at equilibrium. In free solution without collagen, it is estimated that the proteoglycan and GAG aggregates would expand to approximately five times their constrained volume in cartilage (Muir, 1983; Lai et al., 1991). Because it is unlikely that the glycocalyx contains collagen or any other constituent that could limit expansion of the matrix, such a high fixed-charge density as that found in cartilage would not be expected. Therefore, for $c_{\text{blood}} = 0.14$ mol/l, a physiological upper bound on ξ_0 consistent with other mucopolysaccharide structures is $\xi_0 < \sim 1$.

Clearly, this falls well below the range in which ξ_0 would need to be to account for the prolonged diffusion times of anionic molecular tracers reported by Vink and Duling (2000). In addition, there is another difficulty in reconciling the results of Vink and Duling (2000) with those of the analysis presented here. For even if $\xi_0 \gg 1$, the model predicts the existence of a dark band in fluorescence intensity where the glycocalyx is located by virtue of the exclusion of the anionic tracers by the layer. In contrast, the results of Vink and Duling (2000) seem to imply that as the diffusion of molecular tracers progresses, the concentration distribution advances through the glycocalyx as a front. If their observation of a front is valid, then it is very likely that the process is highly nonlinear. This is in contrast to the weak nonlinearity of the present model, which was well-approximated by a linearized model. A possible source of nonlinearity may arise if reaction-diffusion kinetics, not accounted for in this model, are superimposed on the relatively simple electrochemical dynamics described here and mediate interactions between anionic molecular tracers and the glycocalyx. One speculation is the possibility that the anionic molecular tracers bind nonspecifically with cationic sites on albumin and other plasma proteins adsorbed to the glycocalyx, and/or that the tracers compete for those sites with the proteoglycan and GAG aggregates constituting the glycocalyx.

Experimental implications of the model

In light of the foregoing discussion, it seems unlikely that the glycocalyx fixed-charge density can be inferred from diffusion experiments involving anionic molecular tracers such as those performed by Vink and Duling (2000). However, the model does suggest an alternative approach to experimentally extracting material properties of the layer. In particular, the voltage gradients induced by the charge imbalances near the apical end of the glycocalyx suggest useful experiments along the lines of those done by Masaki et al. (2000). Even for a relatively low fixed-charge density, Eq. 43 predicts the existence of a maximum equilibrium voltage difference between the lumen and the glycocalyx ranging between 0.134 and 1.34 mV at 37°C, for $0.01 \leq \xi_0 \leq 0.1$. The presence of such an electric field suggests a method for directly probing the electromechanical properties of the layer. Although it is technically feasible to measure voltages of this magnitude, the practical limitations of using a microelectrode to obtain accurate in vivo measurements of voltage gradients in a 400-nm-thick hydrated gel may be prohibitive. However, modulation of an externally applied electric field might be more plausible, and might offer the possibility of varying the dimension of the glycocalyx in vivo. Because the equations used to derive Eq. 43 are obtained for steady-state conditions, voltage measurements are not subject to uncertainties in the measurements of diffusion times. Furthermore, voltage measurements do not require the use of molecular probes because the voltage depends only on the valence of the free salt and the glycocalyx fixed-charge density. Despite potential technical difficulties, Eq. 43 provides a great incentive to devise such experiments, which would in turn allow direct measurement of the local glycocalyx fixed-charge density without calibration. Finally, Eq. 43 does not depend upon the existence of the extravascular space, so that the geometric assumptions used to derive the diffusion times are unnecessary.

The model suggests yet another approach to estimating the fixed-charge density distribution of the glycocalyx that does not depend upon the transient electrochemical dynamics of the system. The equilibrium distribution of the anionic molecular tracer, given by Eq. 33, or equivalently, by Eq. 51, depends upon ξ_0 and the magnitude, m, of the tracer valence. As we have demonstrated, even if ξ_0 is small, the exclusion factor, given by Eq. 34, can be large if m is sufficiently large (see Figs. 2 and 6). For example, Eq. 34 predicts that if $\xi_0 = 0.01$, a 40% reduction in tracer concentration within the glycocalyx can be achieved if $m = 100$. Thus, if the fluorescence varies linearly with tracer concentration, then the intensity profile from very nega-

tively charged tracers at equilibrium will produce a direct image of $nc_0^F(r)$, according to Eq. 51. Although this does require knowledge of m, it provides an easy way to physically view and quantify the glycocalyx fixed-charge density in vivo.

SUMMARY

A dynamical model of the electrochemical transport of anionic molecules through the capillary glycocalyx has been presented that details the spatiotemporal variations in the concentration field of the diffusing molecules for the axisymmetric case. Numerical and analytical solutions were obtained including a fully analytic eigenfunction expansion that satisfied the linearized equations for a box-shaped distribution of the glycocalyx fixed-charge density. From this solution, closed-form asymptotic expressions were obtained for the first nonzero eigenvalue and the anionic diffusion time that were closely related to the anionic molecular exclusion factor at equilibrium. From the asymptotic analysis, which applies if either $\xi_0 \gg 1$ or m is large, prolonged diffusion times are predicted that are limited by the degree of exclusion of anions from the layer. In either case, if leakage of anionic molecules out of the capillary occurs, diffusion time is seen to vary exponentially with m and in inverse proportion to the anionic molecular exclusion factor. It was also found that the diffusion time was nearly independent of the extravascular cavity size, but the electrochemical dynamics and transient response of the system were critically dependent on the presence of such a cavity. Generally, results were found to be relatively insensitive to the precise shape of the glycocalyx fixed-charge density distribution and to the layer thickness.

One of the most important findings of the present study pertains to the electrochemical equilibrium configuration of the glycocalyx and its implications for anionic molecular exclusion. In particular, the analytical work suggests a number of experiments that would offer useful tests of theoretical predictions made by the model under steady-state conditions and provides a means for obtaining an estimate of the glycocalyx fixed-charge density in vivo. Another important implication of the model pertains to the interpretation of recent in vivo findings of Vink and Duling (2000). In particular, the model shows definitively that, for physiological values of glycocalyx fixed-charge density, diffusion times for anionic molecular tracers with $m < 10$ are not significantly influenced by the electrostatic field induced by the glycocalyx; this finding thus eliminates the possibility that such a field is strong enough to account for the observed behavior of anionic molecular transport through the layer reported by Vink and Duling (2000). It seems likely, therefore, that in addition to the electrochemical dynamics described here, more complicated rate-limiting interactions between the anionic tracers and the glycocalyx occur simultaneously, which might take the form of unknown reaction-diffusion kinetics associated with tracer transport through the layer.

The authors gratefully acknowledge K. Ley, A. J. Pearlstein, and R. D. Rabbitt for their careful reading of the manuscript and for their helpful insights and suggestions. The authors also convey their appreciation to D. O. Pushkin for his helpful suggestions regarding the numerical implementation of the finite-difference equations.

Partial support for this work was provided by the Whitaker Foundation (Grant RG-98-0524).

APPENDIX

Asymptotic approximation of λ_1 for multivalent mobile ions

In deriving Eq. 72, it was assumed that the free salt ions were monovalent, i.e., $z^+ = -z^- = 1$. This assumption led to the quadratic equation in c^+ given by Eq. 30. For arbitrary free-ion valences, this equation becomes

$$c^+(0)^{1/z^+ - 1/z^-} = c^+(r)^{1/z^+}\left(c^+(r) - \frac{nF}{z^+B}c^F(r)\right)^{-1/z^-}, \qquad (76)$$

where $c^+(0) = 1$. The root of Eq. 30 was used in Eq. 37 (which is general) to express δ in terms of $c^F(r)$. For arbitrary values of z^+ and z^-, the more general equation will still have a positive real root, $c^+(r)$, depending on $c^F(r)$. Thus, the exclusion factor is a function of the glycocalyx concentration distribution and the ion valences. For convenience, we define f as in the first of Eq. 40, without specifying the functional form of $c^+(r)$ in terms of $c^F(r)$. In general, then,

$$f(r) \equiv \frac{m}{z^+}\ln(c^+(r)) \qquad (77)$$

where it is understood that f ultimately depends only on the concentration distribution $c^F(r)$, because $c^+(r)$ is derived from the root of Eq. 76, which depends only on $c^F(r)$. Using this definition of f, Eq. 39 becomes general. As such, all the analytic work that follows it is still completely valid. In particular, the definition of $\Delta f \equiv f(r_{g+}) - f(r_{g-})$ may be used, and the results of the asymptotic analysis up to Eq. 71 are true for arbitrary valences. Of course, Δf may be calculated directly from the root of Eq. 76. Indeed, Δf may be evaluated explicitly in terms of $c^+(r_{g+})$. Where $c^F(r)$ is insignificant, i.e., where $\xi(r) = 0$, Eq. 76 has the solution $c^+(r) = c^+(0) = 1$, and it again follows that $f(r_{g-}) = 0$. According to Eq. 77, we then have $\Delta f = f(r_{g+}) - f(r_{g-}) = m/z^+ \ln(c^+(r_{g+}))$.

Roots of Eq. 76 were presented earlier for the case of monovalent cations and anions. They can be found analytically for three more cases: when $z^+ = 2$, $z^+ = 3$ (both for $z^- = -1$ and arbitrary ξ_0), or when $\xi_0 \gg 1$ for arbitrary $z^\pm$. Again, these can be used to write an analytic expression for λ_1. For $z^+ = 2$ or 3 (and $z^- = -1$), Eq. 76 can be written as a cubic or quartic polynomial, respectively, each of which has roots expressible in terms of algebraic numbers. We do not give them explicitly here. For $\xi_0 \gg 1$, it is possible to derive a general closed-form asymptotic expression for λ_1, valid for arbitrary z^+ and z^-. If we rewrite Eq. 76 as

$$\left(\frac{c^+(r)}{c^+(0)} - \xi_0\frac{c^F(r)}{c^+(0)}\right)^{-z^+/z^-}\left(\frac{c^+(r)}{c^+(0)}\right) = 1, \qquad (78)$$

we note that, because $-z^+/z^-$ is strictly positive, the first bracket on the left-hand side must nearly vanish wherever $c^F(r)$ is significant and $\xi_0 \gg 1$. In this case (recalling that $c^+(0) = 1$), $c^+(r) \approx \xi_0 c^F(r) = \xi(r)$, so

$f(r_{g+}) = (m/z^+)\ln \xi_0$. Thus, $\Delta f = \ln \xi_0^{m/z^+}$, and so Eq. 71 becomes

$$\lambda_1 \approx \left(\frac{2(1 - r_{ec}^2 + r_g^2)}{\ln(r_{ec}/r_g)(1 - r_{ec}^2)r_g^2}\right)^{1/2} \xi_0^{-m/2z^+}. \qquad (79)$$

It should be noted that Eqs. 72 and 79 agree when $z^+ = 1$ and $\xi_0 \gg 1$. It should further be noted that this asymptotic result is independent of the anionic valence, z^-. Although the physiological relevance of the case where $\xi_0 \gg 1$ is somewhat dubious, the simplicity and generality of Eq. 79 are attractive and might be applicable to in vitro studies at significantly reduced plasma ionic strength.

REFERENCES

Bockris, J. O. M., and A. K. N. Reddy. 1970. Modern Electrochemistry. Plenum Press, New York.

Boyce, W. E., and R. C. DiPrima. 1992. Elementary Differential Equations and Boundary Value Problems. John Wiley and Sons, New York.

Curry, F. E. 1984. Mechanics and thermodynamics of transcapillary exchange. *In* Handbook of Physiology. Cardiovascular System. Microcirculation, Sect. 2, Vol. IV, Pt. 1, Chapt. 8. American Physiological Society, Bethesda, MD. 309–374.

Damiano, E. R. 1998. The effect of the endothelial-cell glycocalyx on the motion of red cells through capillaries. *Microvasc. Res.* 55:77–91.

Damiano, E. R., B. R. Duling, K. Ley, and T. C. Skalak. 1996. Axisymmetric pressure-driven flow of rigid pellets through a cylindrical tube lined with a deformable porous wall layer. *J. Fluid Mech.* 314:163–189.

Desjardins, C., and B. R. Duling. 1990. Heparinase treatment suggests a role for the endothelial cell glycocalyx in regulation of capillary hematocrit. *Am. J. Physiol. Heart Circ. Physiol.* 264:H909–H916.

Fox, J. R., and H. Wayland. 1979. Interstitial diffusion of macromolecules in the rat mesentery. *Microvasc. Res.* 18:255–276.

Henry, C. B. S., and B. R. Duling. 1999. Permeation of the luminal capillary glycocalyx is determined by hyaluronan. *Am. J. Physiol. Heart Circ. Physiol.* 277:H508–H514.

Klitzman, B., and B. R. Duling. 1979. Microvascular hematocrit and red cell flow in resting and contracted striated muscle. *Am. J. Physiol. Heart Circ. Physiol.* 237:H481–H490.

Lai, W. M., J. S. Hou, and V. C. Mow. 1991. A triphasic theory for the swelling and deformation behaviors of articular cartilage. *J. Biomech. Eng.* 113:245–258.

Levick, J. R. 1987. Flow through interstitium and other fibrous matrices. *Q. J. Exp. Physiol.* 72:409–438.

Ley, K., and K.-E. Arfors. 1986. Segmental differences of microvascular permeability for FITC-dextrans measured in the hamster cheek pouch. *Microvasc. Res.* 31:84–99.

Maroudas, A. 1975. Biophysical chemistry of cartilaginous tissues with special reference to solute and fluid transport. *Biorheology.* 12:233–248.

Masaki, K., A. R. McAllister, and D. M. Freeman. 2000. Electrical properties of the isolated mouse tectorial membrane. *Abstracts of the Twenty-third Midwinter Research Meeting of the Association for Research in Otolaryngology.* 204.

Muir, H. 1983. Proteoglycans as organizers of the extracellular matrix. *Biochem. Soc. Trans.* 11:613–622.

Pries, A. R., T. W. Secomb, H. Jacobs, M. B. Sperandio, K. Osterloh, and P. Gaehtgens. 1997. Microvascular blood flow resistance: role of endothelial surface layer. *Am. J. Physiol. Heart Circ. Physiol.* 273: H2272–H2279.

Reif, F. 1965. Fundamentals of Statistical and Thermal Physics. McGraw-Hill, New York.

Secomb, T. W., R. Hsu, and A. R. Pries. 1998. A model for red blood cell motion in glycocalyx-lined capillaries. *Am. J. Physiol. Heart Circ. Physiol.* 274:H1016–H1022.

Stace, T. M. 1999. An electrochemical model of the diffusion of charged molecules through the capillary glycocalyx. Honor's Thesis, University of Western Australia, Perth.

Vink, H., and B. R. Duling. 1996. Identification of distinct luminal domains for macromolecules, erythrocytes, and leukocytes within mammalian capillaries. *Circ. Res.* 79:581–589.

Vink, H., and B. R. Duling. 2000. The capillary endothelial surface layer selectively reduces plasma solute distribution volume. *Am. J. Physiol. Heart Circ. Physiol.* 278:H285–H289.